Available online at www.sciencedirect.com
ScienceDirect
Icarus 187 (2007) 69–86
ICARUS
www.elsevier.com/locate/icarus

Comparison of the composition of the Tempel 1 ejecta to the dust in Comet C/Hale–Bopp 1995 O1 and YSO HD 100546

C.M. Lisse [a,*], K.E. Kraemer [b], J.A. Nuth III [c], A. Li [d], D. Joswiak [e]

[a] *Planetary Exploration Group, Space Department, Johns Hopkins University Applied Physics Laboratory, 11100 Johns Hopkins Rd, Laurel, MD 20723, USA*
[b] *AFRL/VSBYB, 29 Randolph Road, Hanscom AFB, MA 01731, USA*
[c] *Code 691, NASA Goddard Spaceflight Center, Greenbelt, MD 20771, USA*
[d] *Department of Physics and Astronomy, University of Missouri, Columbia, MO 65211, USA*
[e] *Department of Astronomy, MS 351580, University of Washington, Seattle, WA 98195, USA*

Received 17 April 2006; revised 9 November 2006

Available online 20 December 2006

Abstract

Spitzer Infrared Spectrograph observations of the Deep Impact experiment in July 2005 have created a new paradigm for understanding the infrared spectroscopy of primitive solar nebular (PSN) material—the ejecta spectrum is the most detailed ever observed in cometary material. Here we take the composition model for the material excavated from Comet 9P/Tempel 1's interior and successfully apply it to Infrared Space Observatory spectra of material emitted from Comet C/1995 O1 (Hale–Bopp) and the circumstellar material found around the young stellar object HD 100546. Comparison of our results with analyses of the cometary material returned by the Stardust spacecraft from Comet 81P/Wild 2, the in situ Halley flyby measurements, and the Deep Impact data return provides a fundamental cross-check for the spectral decomposition models presented here. We find similar emission signatures due to silicates, carbonates, phyllosilicates, water ice, amorphous carbon, and sulfides in the two ISO-observed systems but there are significant differences as well. Compared to Tempel 1, no Fe-rich olivines and few crystalline pyroxenes are found in Hale–Bopp and HD 100546. The YSO also lacks amorphous olivine, while being super-rich in amorphous pyroxene. All three systems show substantial emission due to polycyclic aromatic hydrocarbons. The silicate and PAH material in Hale–Bopp is clearly less processed than in Tempel 1, indicating an earlier age of formation for Hale–Bopp. The observed material around HD 100546 is located ∼13 AU from the central source, and demonstrates an unusual composition due to either a very different, non-solar starting mix of silicates or due to disk material processing during formation of the interior disk cavity and planet(s) in the system.

Keywords: Infrared observations; Spectroscopy; Comets, origin; Comets, composition; Solar nebula

1. Introduction

The recent Deep Impact (DI) mission to the Comet 9P/Tempel 1 (T1) allowed unprecedented observations of the pristine nuclear material hidden beneath the processed surface layer in typical comets. On 2005 July 4, a 364 kg impactor spacecraft from DI hit T1 at a relative velocity of 10.2 km s^{-1}, excavating $\sim 10^6$ kg of material that was observed by the instruments on the DI flyby spacecraft (A'Hearn et al., 2005), as well as in the mid-infrared (IR) by the Spitzer Space Telescope (Werner et al., 2004; Lisse et al., 2006). The presence of abundant water ice in the ejecta (Sunshine et al., 2006), the minimal temperature excursion seen for the excavated dust (Groussin et al., 2007), and the arguments of Melosh (1989) on impact cratering indicate that the bulk of material released from T1 due to DI was gently removed. It may in fact have been emitted in a process similar in intensity to emission mechanisms observed in Comet C/1995 O1 (Hale–Bopp). Fig. 1 compares the mid-IR spectrum of the ejecta to that of the ambient coma (Lisse et al., 2006) taken with Spitzer's Infrared Spectrograph (IRS; Houck et al., 2004) and to that of Hale–Bopp (HB) taken with the Short Wavelength Spectrometer (SWS; Leech et al., 2003) on the Infrared Space Observatory (ISO; Kessler et al., 2003). Comparison of the two

* Corresponding author. Fax: +1 240 228 8939.
E-mail address: carey.lisse@jhuapl.edu (C.M. Lisse).

0019-1035/$ – see front matter
doi:10.1016/j.icarus.2006.11.019

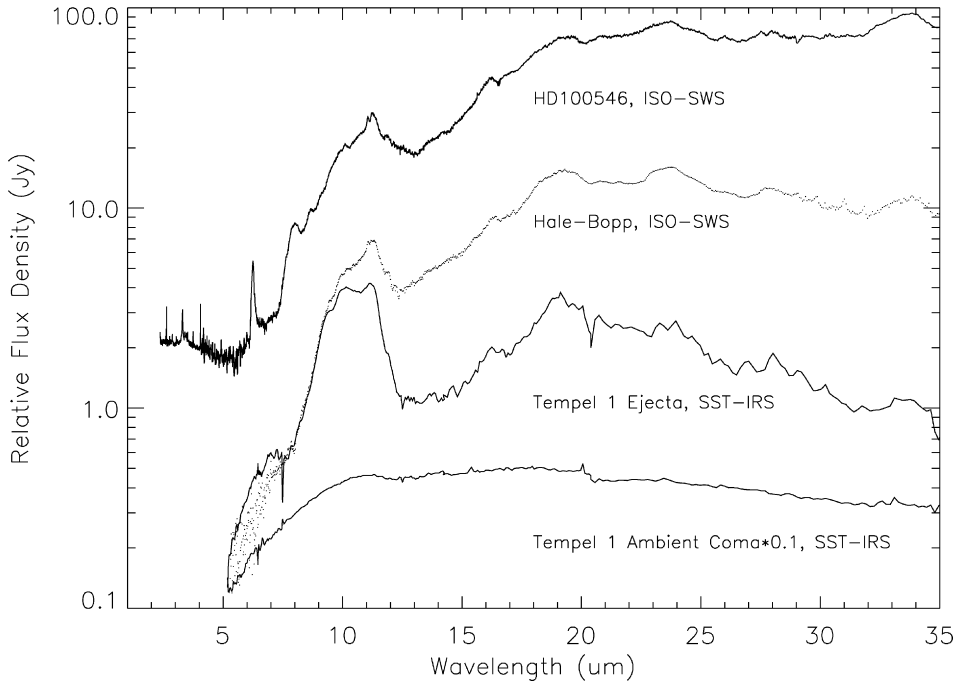

Fig. 1. *Spitzer 5–35 μm spectra of Tempel 1*. From bottom to top, spectrum of the ambient coma, taken 23 h before impact; spectrum of the ejecta at $i + 0.67$ h after impact; ISO spectrum of C/Hale–Bopp (after Crovisier et al., 1997); ISO spectrum of YSO HD100546 (after Malfait et al., 1998). The spectra have been divided by factor of 10, 1, 2.7, and 10 for ease of presentation. Note the logarithmic scale, and the sharper resolution of features in the Tempel 1 ejecta spectrum vs the Hale–Bopp and HD 100546 spectra. It is this increased feature resolution + Spitzer's high spectral sensitivity (compare the error bars in the emissivity plots of Figs. 2–4) that allows the much improved compositional determination of the material in Comet 9P/Tempel 1 as compared to any other comet, including C/Hale–Bopp (after Lisse et al., 2006). The discontinuities in the IRS spectra at 7.5 and 20.5 μm are instrumental artifacts due to slight mismatches in the spectra from the different IRS modules.

comets shows numerous points of similarity, although the T1 spectrum has more structure in its spectrum than HB.

The 1995–1996 apparition of Comet HB, with its strong outflow of small, solid dust (Williams et al., 1997; Lisse et al., 1999; Harker et al., 2002), provided a "natural" IR spectroscopy experiment for ISO to observe. The amount of large particulate material (>10 μm) was more abundant than in the T1 ejecta, leading to a smaller emission feature to continuum ratio in the HB spectra. On the other hand, there was an abnormally large amount of micrometer- and sub-micrometer-sized solid material in the coma to provide a highly featured spectrum (Fig. 1; Crovisier et al., 1997; Lellouch et al., 1998). The presence of this incredibly small and solid dust, in light of the very high rate of emission of material [$\sim 10^{30}$ mol s^{-1} water at 1 AU heliocentric distance (Biver et al., 1999, 2002; Dello Russo et al., 2000); 10^4 kg s^{-1} dust (Li and Greenberg, 1998; Lisse et al., 1999; Jewitt and Matthews, 1999)], begs the question of whether the type of dust normally emitted by comets (Huebner and Benkoff, 1999; Lisse et al., 2002) was altered by the violence of the outflow. Alternatively, the dust from HB may have been unusually volatile rich and fragile, although dust-to-gas ratio estimates for the comet are some of the highest recorded, ∼3–7. Toth and Lisse (2006) argue that Hale–Bopp is rotationally unstable, with centrifugal forces exceeding the shear strength of the nuclear material, leading to large deep cracks in the body and exposure of deep, volatile-rich interior material to solar insolation.

None of the previously published models for the solid material emitted by HB fit the IRS observations of the material excavated from T1 at the 95% confidence level (C.L.; Lisse et al., 2006). In this paper, we briefly recap the new compositional model from the DI–Spitzer observations, focusing on the sanity checks and correlations applied to test the physical reasonableness of the results. We then revisit the ISO spectrum of HB using the new model. We find that the spectra of both comets can be well fit using a compositional model with minimal assumptions based on thermal emissivity measurements of powdered mineral specimens.

The next step is to extend the model to other systems dominated by comet-like material. Here, we present a model for the ISO spectrum of HD 100546 (HD), a ∼10 Myr old Herbig Be9 V star which has often been compared to HB and other comets (e.g., Waelkens et al., 1997). The age of HD corresponds to the era in which planetesimals and planets were formed in the Solar System, and recent work by Liu et al. (2003) and Grady et al. (2005) has demonstrated disk clearing inside 13 AU, most likely due to planet formation. We can easily fit the observed HD spectrum with the DI–Spitzer model as well.

In this paper, we show that the three objects have similar IR spectra due to the presence of common fundamental building blocks of planetary systems (silicates, water, amorphous carbon, carbonates, sulfides, PAHs), but that under closer examination they also have significant differences. We then go on to show that HD resembles HB more than T1 in its dust composition, mean temperature, and size distribution. From this, we deduce that the time of formation, more than location of formation, has the strongest effect on the observed differences

and put T1 into context as a body formed relatively late in the history of the early Solar System. Finally, we speculate from the observed compositional trends on possible new avenues of research to be followed in comparative mineralogy when modeling the plethora of new Spitzer IRS comet and exo-system spectra.

2. Deep Impact and the Tempel 1 dust model

The Spitzer IRS observed T1 on 2–24 July 2005. The 5–35 μm spectra were taken prior to, during, and after the Deep Impact encounter, which occurred when T1 was 1.51 AU from the Sun. The material that was ejected from depths as large as 30 m was pristine and largely unaltered, due to the weakness of the cometary material and the low escape velocity ($\sim$1 m s^{-1}) from the cometary surface (A'Hearn et al., 2005). At the same time, it was de-aggregated from loosely held fractal particles into individual sub-fractal components (A'Hearn et al., 2005; Lisse et al., 2006; Sunshine et al., 2006). The observed material had cooled from effects due to the impact within minutes, and the separation of the ejecta from the ambient coma dust was cleanly made. The resulting highly structured spectrum of the ejecta shows over 16 distinct spectral features at flux levels of a few Janskys (Fig. 1) that persisted for more than 20 h after the impact.

To determine the mineral composition of T1 from the IRS spectra, we applied a model based on measured thermal infrared emission spectra for micrometer-sized particles of over 80 mineral species. Details of the dust model are described in the Supplementary online material for Lisse et al. (2006). This model has limited input assumptions while simultaneously minimizing the number of model parameters. Model solutions were found by a direct search through (composition, temperature, size distribution, porosity) phase space. Acceptable models for the IRS spectra were required to have $\chi^2_\nu < 1.13$ for 325 degrees of freedom at the 95% C.L. The phase space search excluded the vast majority of mineral species from the T1 ejecta. Emission signatures due to Ca/Fe/Mg-rich silicates, carbonates, phyllosilicates, water ice, amorphous carbon, and sulfides were definitively found (Fig. 2 and Table 1; Lisse et al., 2006).

To ensure the robustness of the T1 ejecta modeling, a number of validation checks were applied:

1. All detected materials are associated with major species found in the Interplanetary Dust (IPD) observational databases (Bradley, 2002, 2003; Hörz et al., 2000) and in previous observations of cometary and YSO dust (Bregman et al., 1987; Hanner et al., 1994, 1998; Wooden et al., 1999, 2000).
2. The elemental abundances derived for the observed refractory material are consistent with Solar System abundances.
3. The resulting particle size distribution agrees closely with measurements by the DI instruments (Sugita et al., 2005; Harker et al., 2005; Sunshine et al., 2006).
4. The derived dust temperature is consistent with the temperature measured by the DI High Resolution Instrument (HRI) IR spectrometer (Groussin et al., 2007) and by the NASA Infrared Telescope Facility SpeX instrument (Fernandez et al., 2007).
5. The T1 model results are consistent with the Halley flyby evidence for silicates, water, sulfides, and carbonates to the limit of their sensitivity (cf. Clark et al., 1987; Jessberger et al., 1988), as discussed in Lisse et al. (2006). The CHON particles detected in the Halley flybys ($\sim$25% by number) are identified with the dark amorphous carbon component ($\sim$10% by surface area in the T1 ejecta) used here.
6. Comparison of the compositional results to the preliminary mineralogy results from the Stardust mission (cf. Brownlee et al., 2006a, 2006b; Joswiak and Brownlee, 2006; Zolensky et al., 2006) finds consistency with the refractory species in the T1 model, at the gross level. In the small number of Stardust terminal particles examined to date, evidence for Mg- and Fe-rich olivines, as well as Mg-, Fe-, and Ca-rich pyroxenes were found. Glassy silicates and carbon were abundant, as were metal sulfides. (It must be noted that there are some differences between the T1 model and the Stardust initial findings for the simple terminal particles, as there is no evidence to date of carbonates or phyllosilicates in the preliminary examinations of the samples returned from Wild 2, and the metal sulfides appear most like a non-terrestrial mixture of pyrrhotite ($Fe_{1-x}S$) and pentlandite (FeNiS). On the other hand, the Stardust initial analyses have shown a high degree of particle to particle variation, and a large fraction of the deposited material is found heated, altered and intermixed with the silicate based aerogel capture medium, complicating the analysis of the bulk of the deposited material. Careful study of the systematic effects in the sample return should help solve many of these problems of interpretation, but it is not clear at the time of this writing if issues of small number statistics, hot sample collection into aerogel, collection of mainly surface mantle (and thereby altered) material, or samples from a substantially younger comet are important for the comparison. [For more discussion on these points, see Section 5.4.])

The new modeling presented here allows us to get beyond the classical olivine–pyroxene–amorphous carbon composition to the second-order, less emissive species like water, sulfides, PAHs, phyllosilicates, and carbonates. On the other hand, there are limitations to the method. There is no petrological or isotopic information, and the results returned are for bulk averages of the observed systems. For example, only very abundant species with strong emission features (>10% of the silicate emission peaks) will be detectable. Alumina (Al_2O_3) and hibonite ($CaAl_2O_6$), extremely stable oxides of aluminum, were not definitively detected in the T1 ejecta even though they are known minor constituents of the pre-solar grain population found in interplanetary dust particles (IDPs). Also, in order to cover the large phase space of possible minerals present, we assume a linear mix of the extreme endstates of the mineral each mineral system, and a linear shift in the band positions and strengths between the endstates; e.g., we linearly adjust the balance of forsterite (Fo100, or $MgSi_2O_4$) and fayalite (Fo100,

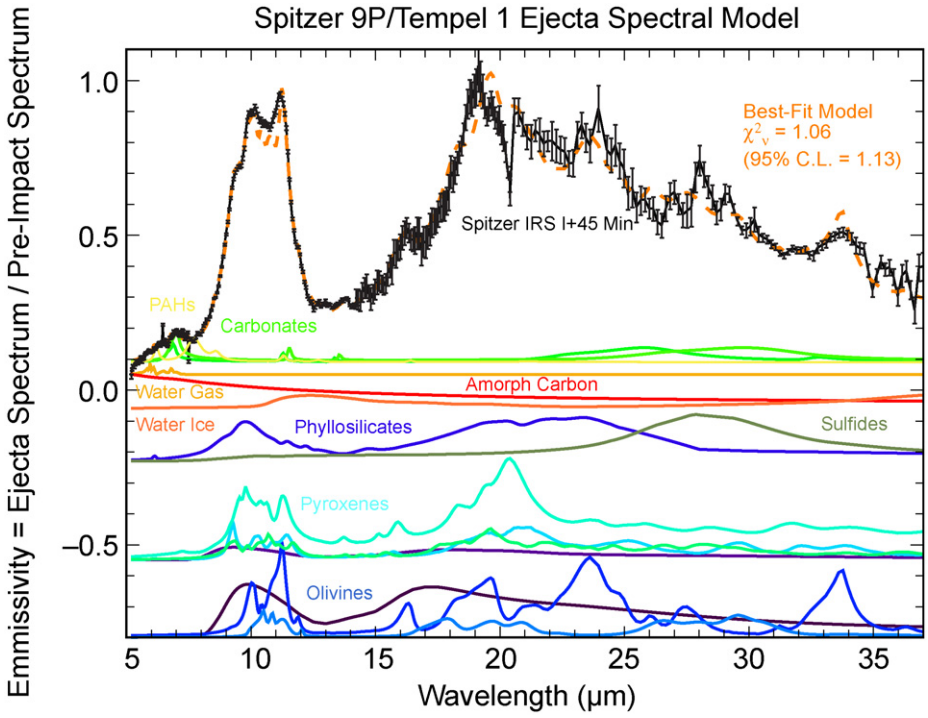

(a)

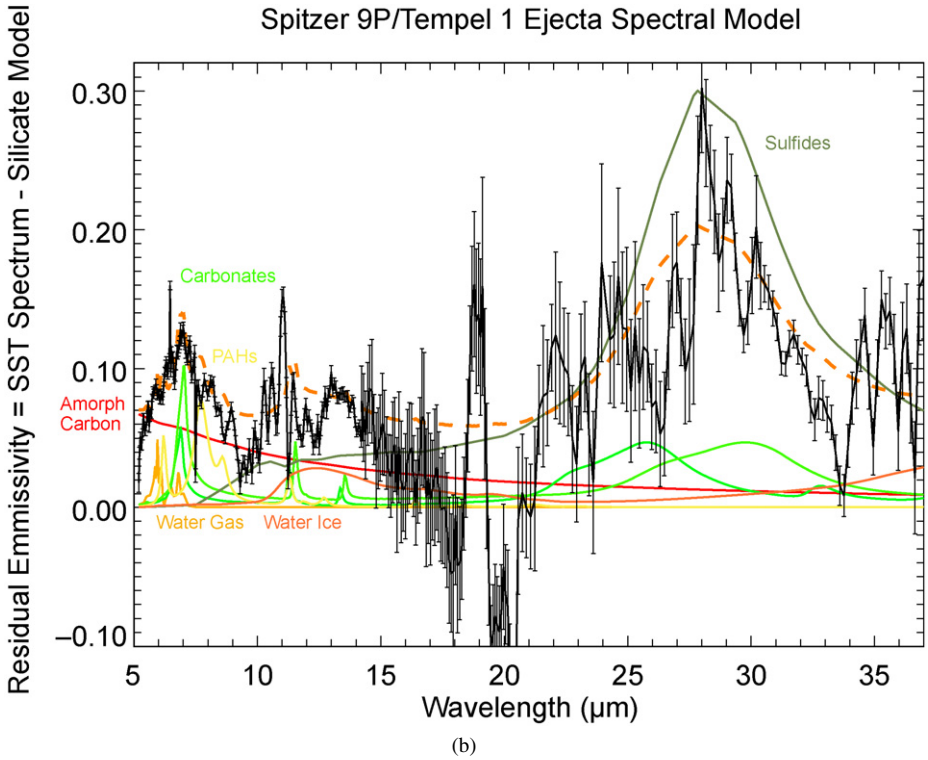

(b)

Fig. 2. *Emissivity spectrum for the Tempel 1 ejecta, at impact + 45 min, showing the individual components of the dust that create the observed emission.* (a) Total spectrum. The comet was 0.75 AU from Spitzer and 1.51 AU from the Sun at the time of observation. The vertical scale is linear to emphasize the closeness of the model fit. Black: SST ejecta spectrum divided by the pre-impact spectrum. Error bars are $\pm 2\sigma$. Orange dashed line—best-fit model spectrum. Colored curves—emission spectra for the constituent species, scaled by the ratio $B_\lambda(T_{\text{dust}}(a)_i)/B_\lambda(T_{\text{post-impact}})$, with $T_{\text{post-impact}} = 390$ K, and offset for clarity. Purple—amorphous silicates of pyroxene or olivine composition. Light blue—crystalline pyroxenes: ferrosilite, diopside, and orthoenstatite, in order of 20 μm amplitude. Dark blue—crystalline olivines, forsterite and fayalite, in order of 20 μm amplitude. Red—amorphous carbon. Deep orange—water ice. Light orange—water gas. Yellow—PAHs. Bright green—carbonates: siderite and magnesite, by order of 7 μm emissivity amplitude. Olive green—sulfides, represented here by niningerite. Blue—phyllosilicates (near the sulfides), represented here by the smectite nontronite. (b) Spectrum after subtraction of the best-fit silicate components. The non-silicate species best-fit emission curves have been overlaid, scaled by a factor of 2. The sharp residual at 19–20 μm is due to a poor match of our forsterite emission spectrum to the data. We see this mismatch for all three systems. (Both figures copyright Lisse et al., 2006.)

Table 1
Composition of the best-fit model to the SST IRS Tempel 1 ejecta spectrum

Species	Weighted surface area	Density ($g\,cm^{-3}$)	M.W.	N_{moles} (rel.)	Model T_{max} (K)	Model χ^2_ν if not included
Olivines						
Amorph olivine ($MgFeSiO_4$)	0.17	3.6	172	0.35	340	5.92
Forsterite (Mg_2SiO_4)	0.31	3.2	140	0.70	340	4.28
Fayalite (Fe_2SiO_4)	0.086	4.3	204	0.18	340	1.40
Pyroxenes						
Amorph pyroxene ($MgFeSi_2O_6$)	0.041	3.5	232	0.06	340	1.38
Ferrosilite ($Fe_2Si_2O_6$)	0.33	4.0	264	0.50	295	9.30
Diopside ($CaMgSi_2O_6$)	0.115	3.3	216	0.18	340	1.86
Orthoenstatite ($Mg_2Si_2O_6$)	0.10	3.2	200	0.16	340	1.70
Phyllosilicates						
Smectite nontronite $Na_{0.33}Fe_2(Si,Al)_4O_{10}(OH)_2{\cdot}3H_2O$	0.14	2.3	496	0.07	340	3.76
Carbonates						
Magnesite ($MgCO_3$)	0.030	3.1	84	0.11	340	1.30
Siderite ($FeCO_3$)	0.051	3.9	116	0.17	340	1.83
Metal sulfides						
Niningerite ($Mg_{10}Fe_{90}S$)	0.15	4.5	84	0.92	340	2.51
Water						
Water ice (H_2O)	0.049	1.0	18	0.27	220	1.40
Water gas (H_2O)	0.028	1.0	18	23.7	220	1.22
'Organics'						
Amorph carbon (C)	0.068	2.5	12	1.45	390	13.3
PAH ($C_{10}H_{14}$)	0.039	1.0	⟨178⟩	0.022	N/A	1.58

Note. $N_{moles}(i) \sim$ density(i)/molecular weight(i) × surface area weighting(i); ±10% errors on the abundances (2σ). Total best-fit model $\chi^2_\nu = 1.06$. LTE at 1.51 AU $= 230$ K. Table from Lisse et al. (2006).

or $Fe_2Si_2O_4$) to fit the observed spectrum, allowing us to determine the total number of each atom present, but cannot distinguish between the presence of Fo50 ($FeMgSi_2O_4$) and a 50–50 mix of (Fo100 + Fa100). The values in the compositional tables should be interpreted in this way. We also cannot distinguish easily between "glassy silicate of non-stoichiometric but near olivine (or pyroxene) composition" and "amorphous silicate of olivine (or pyroxene) composition" and so we assume the presence of stoichiometric glasses when modeling the glassy silicates.

Despite these limitations, at this point in time we are able to determine the overall amounts of the different classes of material (olivines, pyroxenes, sulfides, water, etc.) and the bulk elemental abundances for the most abundant atoms. Applying the model, with strong checks of its validity, has great potential for interpreting new mid-IR spectra of distant dusty systems like YSOs, debris disks, and PNs. We also expect to update and improve the compositional model presented here, with its linear sum of pure mineral end members, by testing, vs the T1 ejecta emission spectrum, a more precise mineralogical and chemical formulation based on aggregate Stardust measurements once they are available in the next 3 to 5 years.

3. Modeling results for Comet Hale–Bopp

The 2.4–45 μm ISO spectrum of HB obtained by Crovisier et al. (1997, 2000) on 7 October 1996 (heliocentric distance $r = 2.8$ AU, geocentric distance $\Delta = 3.0$ AU) has previously been modeled by others (e.g., Malfait et al., 1998; Wooden et al., 1999, 2000; Min et al., 2005). In those analyses, though, the authors typically focus on a specific species or lack definitive measures of the basic nature and makeup of the observed dust. A mix of material consisting of olivines, amorphous carbon, native iron, and/or water ice is usually assumed, often without regard to cosmic or Solar System abundances. Two separate particle size distributions are often used for the continuum and spectral features, and a run of temperature and density is found as a solution. Inferences are then drawn concerning the dominant physical processes in the system from the observed distributions. Spectral features which cannot be fit, including emissions from carbonates, PAHs, sulfides and phyllosilicates, are left as a residual, and rarely if ever is the chi-squared statistic for the presented best-fit model given. Here we revisit this modeling, using the new results on cometary composition found by modeling the T1 ejecta, and a statistically robust fitting method. The higher feature-to-continuum ratio and sensitivity in the Spitzer spectrum allowed for the detection and identification of more materials than were previously found in the HB data alone. This accurate determination of the composition of the T1 material enables us to revisit the HB spectrum and remove some of the ambiguities produced by the presence of large, optically thick dust grains in the HB coma.

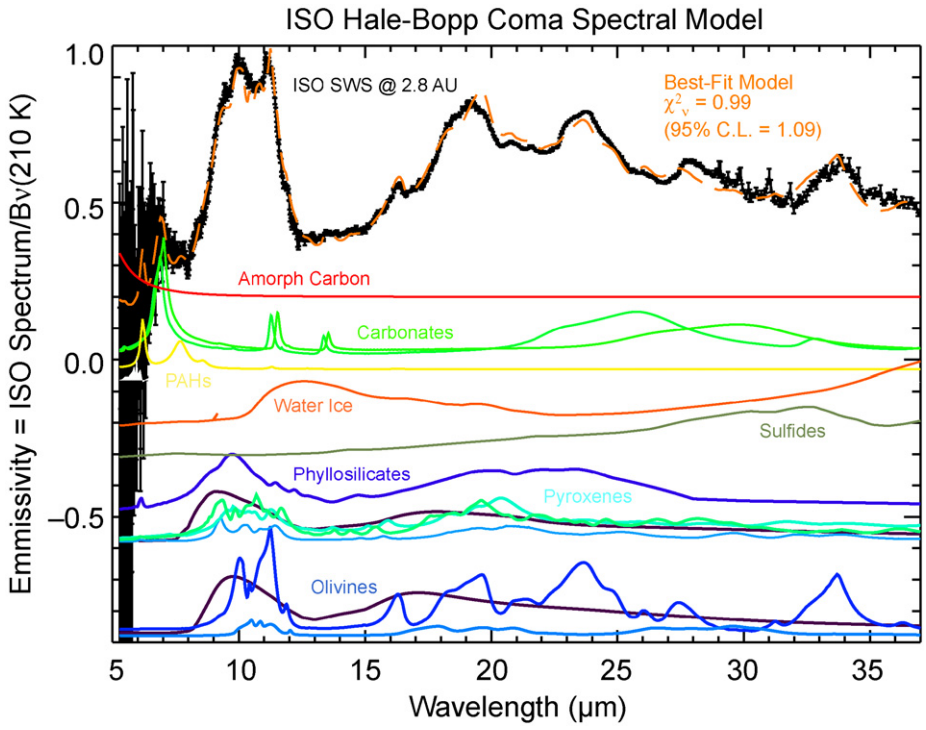

(a)

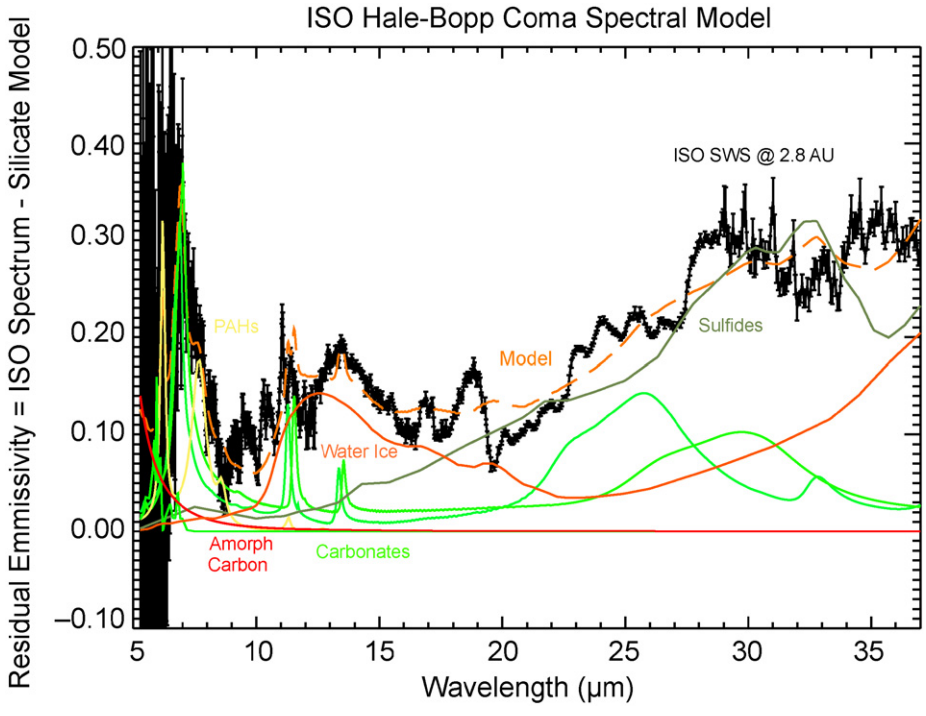

(b)

Fig. 3. (a) *Emissivity spectrum for the Hale–Bopp naturally emitted coma, as measured at 2.8 AU from the Earth and ISO*. Error bars are $\pm 2\sigma$. Black—ISO coma spectrum, divided by a 210 K blackbody. The colored curves have the same sense as in Fig. 2. Except for Fe-rich olivine and water gas, the entire suite of species found in the Tempel 1 ejecta is also found in the Hale–Bopp coma. (b) Spectrum after subtraction of the best-fit silicate components, as in (a).

3.1. Size distribution and mass

The new modeling was greatly aided by the determination that the particle size distribution of the HB coma is dominated by small, solid, icy grains with a power law size distribution $dn/da \sim a^{-3.6 \text{ to } 4.0}$ (cf. Williams et al., 1997; Lisse et al., 1999; Harker et al., 2002), and porosity ~0. Using this PSD range, we find the total mass associated with the spectrum is approximately 2×10^9 kg, three orders of magnitude more than was observed in the T1 ejecta. Even so, this is still small compared

with the amount of dust seen in the whole coma + tail structure of HB ($\sim 10^{11}$ kg; Lisse et al., 1998; Lisse, 2002). The difference is due to two effects: the small angular size of the ISO SWS spectrometer beam versus the very extensive HB coma + tail; and the fact that the HB coma, unlike the comae of almost any other comet, was optically thick near the nucleus due to its huge rate of emission of material.

3.2. Temperature

The best-fit simple blackbody to the continuum has a temperature of 210 K. From our more detailed T1 compositional model, we find the temperature of the smallest dust particles (0.1–1.0 μm), which superheat above local thermal equilibrium (LTE), is ∼220 K for the olivines, 190 K for the pyroxenes, and 410 K for the amorphous carbon. The largest particles included in the model, 1000 μm, are set to $T_{\rm LTE} = 282/\sqrt{(2.8\ {\rm AU})} = 169$ K, and dust of intermediate size is scaled between the two extremes (Lisse et al., 2006). We find the best-fit temperature of the water ice and gas, cooled by the heat of sublimation below LTE, to be ∼150 K, regardless of particle size.

We note here an important point in analyzing the data: the scattered sunlight from the coma of HB must be carefully fit and removed before modeling the data. Otherwise the comet appears to have a huge super-thermal continuum. For the large majority of comets, the scattered light component would be negligible longwards of ∼3 μm. However, the albedo of HB's dust was so high (∼40% vs ∼8% for T1's ambient coma) and the comet was observed relatively far from the Sun (∼2.8 AU vs a more typical 0.7–1.5 AU) with cold coma dust, that the scattered light component was significantly enhanced and an important component of the measured 5–10 μm radiation.

3.3. Composition

With compositional phase space for comet-like material now defined robustly by the DI results, and porosity and size distribution given by the literature, we solve iteratively for the relative amount of each species while demanding good agreement with the measured ISO spectrum. We find that there is no need to make the ad hoc assumption of two separate particle size distributions, hollow spheres, long needles, or an unusual mineral composition. The same material that yields the sharp spectral features also provides the continuum, from its larger, optically thick pieces. In fact, the number of materials making up the majority of the coma dust of HB is fewer than for T1.

The results of fitting the SWS spectrum of HB taken at 2.8 AU are given in Table 2, Fig. 3a (full spectrum), and Fig. 3b (residuals after the dominant silicate and phyllosilicate best-fit model is removed). The best-fit model had a $\chi^2_\nu = 0.99$; the last column of the table indicates the change in χ^2_ν if a particular species is not included in the model. Fig. 3 shows the ISO data with best-fit spectral model superimposed, as well as the spectrum of each contributing species broken out separately. In contrast to T1 (Figs. 2, 5), there is no Fe-rich olivine (fayalite, Fe_2SiO_4). There is also more amorphous olivine relative to Mg-rich crystalline forsterite (Mg_2SiO_4), as was found by Wooden et al. (1999). Total pyroxenes (e.g., $MgFeSi_2O_6$), both crystalline and amorphous, are present in about the same amount as for T1, consistent with the results of Wooden et al. (1999, 2000). The fraction of amorphous pyroxene material is much higher in HB than T1.

Phyllosilicates (as represented by the smectite nontronite, $Na_{0.33}Fe_2(Si,Al)_4O_{10}(OH)_2{\cdot}3H_2O$) seem slightly enhanced and carbonates (magnesite $MgCO_3$ and siderite $FeCO_3$) extremely enhanced, by a factor of 3, relative to T1. The latter statement depends strongly on the veracity of the ISO SWS 5–8 μm data where the error bars are large. However, the chi-squared fitting routine used to derive the composition takes these effects into account and omitting the carbonate from the model more than doubles χ^2_ν (Table 2). The sulfide emission feature (niningerite [Mg, Fe^{2+}]S) is similar in the two comets, although the best-fit ningerite composition is $Fe_{0.9}Mg_{0.1}S$ for HB (and HD, see Section 4.2) rather than the $Fe_{0.5}Mg_{0.5}S$ found for T1. The water ice signal is much larger in HB than for T1 because HB was beyond the ice line at the time of observation. Water ice is thus more stable, and the effective temperature we find for the water ice, ∼140 K, is near the LTE temperature.

The detection of PAHs in the comet deserves some discussion. We find that in the best-fit HB model, there is about twice as much PAH material per mole of dust than was found for T1. For such an active comet with strong signatures of organic species such as methane, ethane, and methanol (Biver et al., 1999; Bockelée-Morvan et al., 2000) and a significant amount of amorphous carbon, the presence of PAHs was not unexpected. The 3.3 μm PAH feature was tentatively detected amongst OH and H_2O lines in a few comets, P/Halley, Levy, and Brorsen–Metcalf (Encrenaz et al., 1988; Bockelee-Morvan et al., 1995), and fluorescence features attributed to aromatics were also tentatively detected in the near-UV in P/Halley (Moreels et al., 1994; Clairemidi et al., 2004). However, the detection of PAHs in HB disagrees with previous determinations for this comet (Crovisier et al., 2000). The difference in the current work is the proper assignment of the compositional materials making up the coma dust and the careful removal of the dominant silicate and amorphous carbon emission from the spectra, allowing detection of the secondary emitters. Also, the T1 results showed that ionized PAHs dominated in the ejecta (Fig. 2b), implying an ionization timescale of less than 1000 s, so that we can expect the HB coma PAHs to be ionized as well. Detection of PAHs using the feature at 3.29 μm would therefore also be problematic, as the amplitude of this emission is decreased by about a factor of 20 compared to ionized PAHs. The 3.29 μm flux we estimate from our T1 model, 0.02 Jy, corresponds to one-fifth the amplitude or about 1σ of the most pronounced PAH emission feature from Comet Levy in Bockelee-Morvan et al. (1995). The PAH signal for HB is about three times as large, or 3σ.

3.4. Elemental abundances

Far and away the most abundant atomic species in the Primitive Solar Nebula (PSN), as in the ISM, was H, followed by He. Heavier and more complex nuclei are much rarer, by orders

Table 2
Composition of the best-fit model to the ISO SWS 2.8 AU Hale–Bopp spectrum

Species	Weighted surface area	Density ($g\,cm^{-3}$)	M.W.	N_{moles} (rel.)	Model T_{max} (K)	Model χ^2_ν if not included
Olivines						
Amorph olivine ($MgFeSiO_4$)	0.18	3.6	172	0.37	220	8.76
Forsterite (Mg_2SiO_4)	0.32	3.2	140	0.73	220	8.17
Fayalite (Fe_2SiO_4)	0.03	4.3	204	0.06	220	1.07
Pyroxenes						
Amorph pyroxene ($MgFeSi_2O_6$)	0.13	3.5	232	0.20	220	4.72
Ferrosilite ($Fe_2Si_2O_6$)	0.11	4.0	264	0.17	190	3.39
Diopside ($CaMgSi_2O_6$)	0.05	3.3	216	0.08	220	1.22
Orthoenstatite ($Mg_2Si_2O_6$)	0.12	3.2	200	0.19	220	3.43
Phyllosilicates						
Smectite nontronite $Na_{0.33}Fe_2(Si,Al)_4O_{10}(OH)_2{\cdot}3H_2O$	0.18	2.3	496	0.08	220	8.15
Carbonates						
Magnesite ($MgCO_3$)	0.15	3.1	84	0.55	220	1.92
Siderite ($FeCO_3$)	0.18	3.9	116	0.60	220	2.20
Metal sulfides						
Niningerite ($Mg_{10}Fe_{90}S$)	0.15	4.5	84	0.80	220	4.95
Water						
Water ice (H_2O)	0.34	1.0	18	1.89	150	8.68
Water gas (H_2O)	0.00	1.0	18	0.00	150	0.99
'Organics'						
Amorph carbon (C)	0.08	2.5	12	1.67	410	1.03
PAH ($C_{10}H_{14}$)	0.14	1.0	⟨178⟩	0.08	N/A	1.50

Note. $N_{moles}(i) \sim$ density(i)/molecular weight(i) × surface area weighting(i); ±20% errors on the abundances (2σ). Total best-fit model $\chi^2_\nu = 0.99$. LTE at 2.8 AU = 169 K.

of magnitude, with the abundance falling rapidly with atomic number Z. Simply put, this is a statistical effect—the more protons and neutrons required to make up a nucleus, the lower the probability the nucleus was formed. There are exceptions to this rule—the metals CNO are enhanced due to their formation in the catalytic CNO cycle, and Fe is super-abundant because it lies at the minimum of the nuclear energy binding curve. Similarly, nuclei with especially stable binding energy configurations—like the even–even nuclei with half-filled or filled nuclear shells—are extra-abundant.

The most abundant atomic species found in primitive solid state materials are H:C:O:Si:Mg:Fe. Nitrogen, while nearly as abundant as C and O, resides mostly in the icy volatile species N_2 and to a lesser extent in NH_3 (e.g., Womack et al., 1992). The bulk of the H, C, and O will be in volatile organic ices and in water ice, but a fraction will be contained in the refractory dust. Since these atomic species are much more abundant than the rock-forming elements Si, Mg, and Fe, they appear in similar numbers. The next tier down of abundant species, Ca:Al:Na, are also important rock-forming elements, and Ca and Al form extremely stable oxides. These are often harder to detect, though, because of their lower solar abundance.

For the T1 model, the relative elemental abundance in the ejected dust are H:C:O:Si:Mg:Fe:S:Ca:Al = 0.42:0.58:3.9:1.0:0.88:0.79:0.29:0.054:$\leqslant$0.085 (for Si = 1.0). For reference, the solar abundance values vs Si are 3.1×10^4:7.6:14.1:1.00:1.05:0.87:0.43:0.063:0.072 (Anders and Grevesse, 1989; Asplund et al., 2005). The Si:Mg:Fe:Ca:Al ratios we find for T1 are consistent with Solar System abundances determined from the Sun and from C1 chondrites (Asplund et al., 2005; Fig. 6). Hydrogen is very deficient, as expected for small primitive bodies' inability to retain solar nebula H_2. Carbon is deficient by a factor of ∼13. Oxygen is less deficient in the dust than carbon, depleted by a factor of ∼3.5, presumably due to its more lithophilic chemistry. Sulfur appears deficient by a factor of 1.5, which suggests that we may not have well characterized the sulfide constituents or that primitive bodies do not efficiently accrete the more volatile sulfur compounds such as H_2S or SO_2 from the nebula.

For the HB model, the relative elemental abundance in the coma are H:C:O:Si:Mg:Fe:S:Ca:Al = 1.6:12:5.3:1.0:1.2:0.86:0.34:0.054:$\leqslant$0.11 (for Si = 1.0). These abundances are generally closer to the solar abundances (Fig. 6) than are those for T1. More H is present in the form of water ice for HB, as some of that volatile fraction was still in the solid phase when the comet was observed at $r = 2.8$ AU where $T_{LTE} = 167$ K. Carbon is not deficient at all. Oxygen is highly deficient, with the balance of atoms contained in the large amount of coma H_2O and CO/CO_2 gas in this most active of modern comets. The Si:Mg:Fe:Ca:Al rock forming element ratios trends are nearly chondritic. Sulfur appears deficient by approximately 30%, suggesting again that we are not well characterizing the sulfide constituents or that comets do not efficiently accrete volatile forms of S. A similar suggestion was made by Lisse et al. (2006) and has been

reinforced by recent Stardust results. Keller et al. (2006) and Zolensky et al. (2006) found pentlandite rather than ningerite to be the majority sulfide phase in the dust of Comet Wild 2.

4. Modeling results for HD 100546

The combined presence of crystalline silicates, phyllosilicates, carbonates, and icy volatiles, and the small amount of PAHs in T1's interior has fundamental implications for the nature of the material incorporated into the comet 4.5 Gyr ago from the PSN. Crystalline silicates formed and PAHs were destroyed within the present orbit of Mercury. Phyllosilicates and carbonates formed in regions of copious water between ∼0.5 and ∼2.5 AU. Icy volatiles were accreted as the comet itself coalesced from these components out beyond the giant planets. One of the most likely possibilities is that there was pronounced mixing in the PSN at the time of the comet's creation (Nuth et al., 2000; Bockelée-Morvan et al., 2002; Lisse et al., 2006). Alternative explanations of the observed chemistry include nebular shockwave heating (Harker and Desch, 2002) and parent body alteration chemistry over the past 4.5 Gyr (Lisse et al., 2006).

With this in mind, it is natural to turn to mid-IR observations of other stellar systems thought to be evolving through the protoplanetary stage, dominated by cometary bodies and comet-like material. In the current paradigm of planetary system formation, the evaporation and condensation of refractory and icy materials takes place in a thick protostellar disk, followed by the settling of solid grains into a thinner disk on a timescale of 10^5 yr. Over the next 10^7 yr, low velocity collisions among the grains result in the accumulation and inward migration of cometary objects, with sizes ranging from mm to km (Weidenschilling, 1997). Planetesimal reservoirs, i.e., protoplanetary disks, consistent with this paradigm have been found around a growing number of young, T Tauri stars (cf. review by Dutrey and Guilloteau, 2004). ISO significantly increased our knowledge of these disks and now Spitzer is adding new insight into this phenomenon (e.g., Forrest et al., 2004; Megeath et al., 2005).

The prototypical YSO system studied for its cometary connections is HD 100546, a Herbig Be9 V star at ∼10 Myr age since formation and 103 pc distance (van den Ancker et al., 1997). Herbig Ae/Be stars are systems of intermediate mass still in their pre-main sequence (PMS) phase of evolution. They have lost most of their surrounding envelope of infalling gas and dust but are not yet fusing hydrogen into helium. Instead they are heated mainly by gravitational contraction and material infall. The ISO SWS spectrum of this system is often compared to that of HB in the literature (e.g., Waelkens et al., 1997; Malfait et al., 1998), and it is used as a laboratory for nebular formation processes because of its apparent primitive makeup and young age (Grady et al., 2001).

4.1. Temperature, mass and size distribution

Here we model the spectral decomposition for the ISO SWS spectrum, as we did for the HB spectrum. The major differences between the YSO and cometary cases are that for HD 100546 (1) a stellar photospheric component must be removed, and (2) a run of material density and temperature vs stellar distance r^* must be addressed. The first issue is relatively straightforward to deal with, and we have used a Kurucz model scaled to short-wavelength photometric and 2–5 μm spectroscopic measurements of the system (Hu et al., 1989; Waelkens et al., 1997) to remove the photospheric contribution. If this is not done properly, then like the effect of the scattered sunlight from HB's coma, the YSO appears to have a huge super-thermal continuum component.

To deal with the second issue, we simplify the problem by assuming that the observed IR emission will be dominated by the hottest and densest material. The best simple blackbody fit to the underlying dust continuum appears to come from a hot region, at $T = 250$ K, similar to the effective temperature of the zodiacal dust as seen from Earth, plus a cooler outer ring with effective temperature $T = 135$ K, as used in the modeling of Bouwman et al. (2003). In contrast, from our detailed T1 compositional model, we find a large range of dust particle temperatures at one astrocentric distance, depending on the particle composition and size influencing its ability to absorb and re-radiate starlight. The best-fit temperature of the smallest dust particles (0.1–1.0 μm) is ∼250 K for the olivines, 190 K for the pyroxenes, 150 K for the water ice and gas, and 410 K for the amorphous carbon. (Water ice and gas tend to "run cold" compared to other dust due to the significant energy absorbed in vaporizing water.) These results indicate an LTE of about 170 K, with the dominant emitters, including both hot silicaceous dust and cold icy dust, all co-located at the same distance from the primary, ∼12–14 AU (assuming $L^* = 22L_{\rm solar}$; van den Ancker et al., 1997; Weinberger et al., 2003). We thus favor a model of the system with the dominant actively emitting material localized in space. Note that 13 AU is the same distance as estimated by Grady et al. (2005) for the inner wall of a cleared cavity in the disk from HST/STIS imaging observations, which would represent the densest and hottest emitting dusty material in the HD system.

Using these dust temperatures, the T1-based dust model works well, with $\chi^2_\nu = 1.07$. The model results are listed in Table 3 and shown graphically in Fig. 4. The best-fit particle size distribution from our modeling, $dn/da = a^{-4.0\pm0.05}$, is steeply weighted towards the small, unaggregated particle sizes. This distribution is steeper even than the $a^{-3.8}$ distribution found for the de-aggregated ejecta produced in the DI experiment (Lisse et al., 2006) and is steeper than all but the most extreme HB models. The total amount of mass associated with the ISO spectrum, estimated by integrating up to the largest detectable particles (20 μm radius), is at least 10^{22} kg, about 1/7 the mass of the Earth's moon. Much larger total masses would be estimated by assuming maximum particle sizes on the centimeter or meter scale, or if the system is optically thick beyond the inner cavity wall. From both the mass and temperature results, it is clear that we are observing a huge amount of circumstellar material spread out over a few AU in this system.

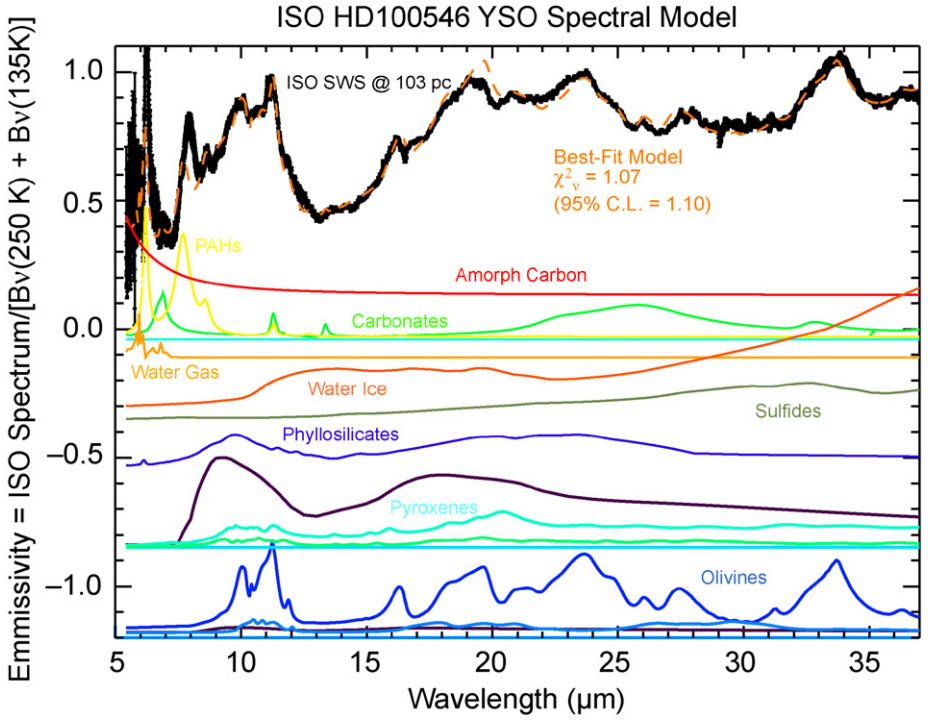

(a)

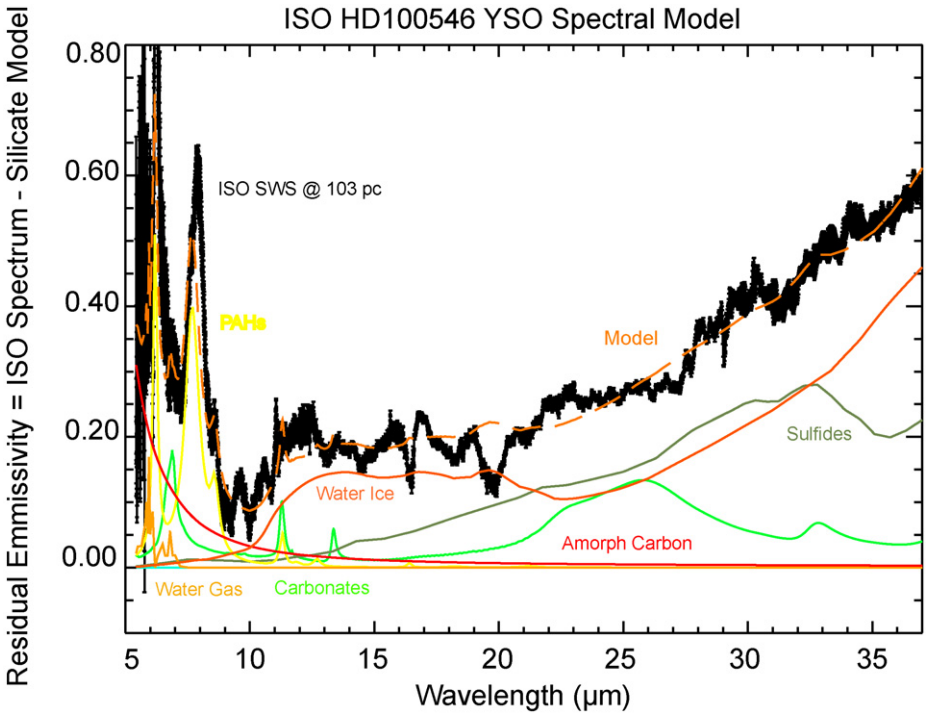

(b)

Fig. 4. *Emissivity spectrum for the ISO HD 100546 spectrum*. (a) Total spectrum. Color scheme is the same as in Fig. 2. Error bars are $\pm 2\sigma$. Black—HD 100546 excess spectrum (i.e., central source removed), divided by a 250 K blackbody. Orange dashed line—best-fit preliminary model, fitting all major features with the 1 temperature assumption. Unlike Tempel 1, the only major olivine species found is Mg-rich and crystalline, while the pyroxenes are limited to Fe-rich crystalline and the amorphous glassy species. No Fe-rich carbonates are detected, and the phyllosilicates are relatively underabundant, while PAHs are superabundant. (b) Spectrum after subtraction of best-fit silicate components, as for (a).

4.2. *Composition*

Applying the same analysis techniques as were used for HB, we obtain a good compositional fit to the HD 100546 ISO SWS spectrum. The results are given in Table 3, Fig. 4a (full spectrum), and Fig. 4b (residuals after the dominant silicate and phyllosilicate best-fit model is removed). What is striking about the resulting overall HD 100546 composition is that it appears

Table 3
Composition of the best-fit model to the ISO SWS HD100546 spectrum

Species	Weighted surface area	Density ($g\,cm^{-3}$)	M.W.	N_{moles} (rel.)	Model T_{max} (K)	Model χ^2_ν if not included
Olivines						
Amorph olivine ($MgFeSiO_4$)	0.00	3.6	172	0.00	250	1.07
Forsterite (Mg_2SiO_4)	0.35	3.2	140	0.80	250	7.36
Fayalite (Fe_2SiO_4)	0.03	4.3	204	0.06	250	1.13
Pyroxenes						
Amorph pyroxene ($MgFeSi_2O_6$)	0.35	3.5	232	0.53	250	20.0
Ferrosilite ($Fe_2Si_2O_6$)	0.15	4.0	264	0.23	190	3.34
Diopside ($CaMgSi_2O_6$)	0.00	3.3	216	0.00	250	1.07
Orthoenstatite ($Mg_2Si_2O_6$)	0.03	3.2	200	0.05	250	1.16
Phyllosilicates						
Smectite nontronite $Na_{0.33}Fe_2(Si,Al)_4O_{10}(OH)_2{\cdot}3H_2O$	0.14	2.3	496	0.07	250	4.03
Carbonates						
Magnesite ($MgCO_3$)	0.08	3.1	84	0.30	250	1.37
Siderite ($FeCO_3$)	0.00	3.9	116	0.00	250	1.07
Metal sulfides						
Niningerite ($Mg_{10}Fe_{90}S$)	0.15	4.5	84	0.80	250	2.37
Water						
Water ice (H_2O)	0.46	1.0	18	2.55	150	9.66
Water gas (H_2O)	0.18	1.0	18	1.00??	150	1.14
'Organics'						
Amorph carbon (C)	0.33	2.5	12	6.8	410	2.51
PAH ($C_{10}H_{14}$)	0.51	1.0	⟨178⟩	0.29	N/A	4.78

Note. $N_{moles}(i) \sim$ density(i)/molecular weight(i) × surface area weighting(i); ±10% errors on the abundances (2σ). Total best-fit model $\chi^2_\nu = 1.07$. LTE at 13 AU = 170 K.

in most respects to be very similar to that of HB, and rather different than the T1 spectrum (Fig. 5). Sulfides, phyllosilicates, and amorphous carbon all seem to be present in roughly the same amounts as seen for the comets. Water is present as both water ice and gas, indicating the observed material is straddling the ice line in the system. A mix of water ice and gas was seen for T1, due to the unusual circumstances of quickly releasing water ice at 1.51 AU from the impact, but there is abundant evidence that the ice began rapidly subliming (e.g., Küppers et al., 2005; Sunshine et al., 2006). For HB, only water ice was found, as expected for a comet at 2.8 AU from the Sun, beyond the ice line. Compared to total normalized number of moles of material found, the relative amount of PAHs in the two systems is found to be the same ($\sim 2 \times 10^{-2}$) and is about a factor of 25 larger than the PAH abundance in T1. The main difference between HD and HB is the super abundance of amorphous pyroxene and absence of amorphous olivine. Also, carbonates are present as only the Mg-rich component, at about one-fifth the abundance seen in HB and about one-half the abundance found in T1.

The presence of abundant forsterite, water ice, and PAHs agrees with the findings of Malfait et al. (1998) and Bouwman et al. (2003) but the presence of sulfides, crystalline pyroxenes, and the lack of FeO do not. The relative amount of phyllosilicate and carbonate is similar to what is seen in the comets, suggesting these species were also present in the PSN.

4.3. Elemental abundances for HD 100546

The relative elemental abundances derived for the HD 100546 nebula are H:C:O:Si:Mg:Fe:S:Ca:Al = 3.0:8.4:4.1:1.0:1.1:0.74:0.52:0.011:⩽0.07 (for Si = 1.0). Compared to the HB coma dust, which is the closest of the 3 systems to solar abundances, there is more H present, in the form of PAHs. The other major H reservoir, water ice, has about the same relative abundance in both systems. Oxygen is markedly deficient compared to the solar value, as for T1 and HB. In contrast, the C abundance is approximately that expected for a solar abundance with some carbon ($\sim 1/3$) found in gaseous species. Si and Mg are close to the solar ratios; Fe is decreased in abundance by 16%, a value that is within the uncertainties of the abundance estimates. The Ca abundance is markedly low vs solar and the two comet systems. The S component, as for T1 and HB, is low by about 30% from what would be expected for a solar abundance star.

5. Discussion

5.1. Temperature and mass of the 3 systems

The temperature of the T1 ejecta was ∼340 K, as expected for dust heated by sunlight at 1.5 AU, but very unlike the temperatures (>100 K) in its region of formation (r_h = 50–200 AU). The temperatures of the observed dust in the disk of HD 100546 (135–250 K) and the coma of HB (∼200 K) are very similar, close to the sublimation temperature of wa-

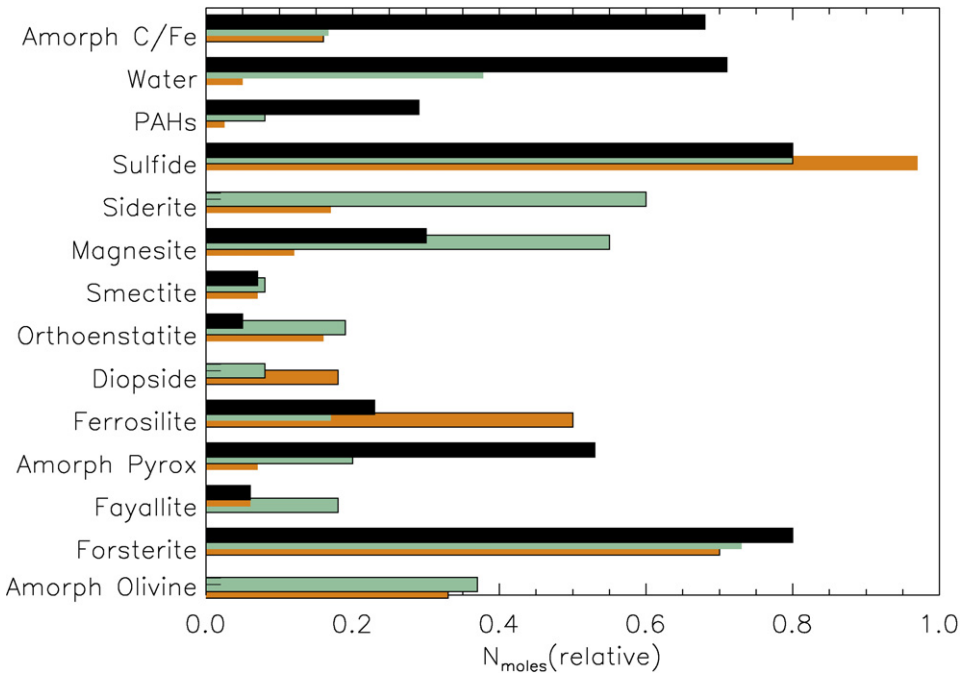

Fig. 5. *Relative mineral abundances for the 3 systems*. Tempel 1 is given in orange, Hale–Bopp is denoted by blue, and HD 100546 by black. The water (gas + ice) abundances have been divided by a factor of 5 and the amorphous carbon abundances by a factor of 10 for ease of presentation.

ter ice. The material observed in HD 100546 corresponds to the material that was incorporated into planetesimals in the inner giant planet region and into the outer main belt asteroids. HB, an Oort cloud comet, could very well have been formed in a similar region of the PSN. All 3 systems show evidence for fine water ice particles, a marker for "gentleness" of the processing of the observed material. None of the 3 systems was warm enough, nor did the DI impact impart sufficient energy to the cold ejecta (A'Hearn et al., 2005; Lisse et al., 2006) to create any large-scale changes in the refractory dust materials, although the some of the more volatile icy materials may have been driven off, and some of the water present vaporized.

The observed dust masses of the three objects vary widely. From smallest to largest, we observed $\sim 1 \times 10^6$ kg of T1 ejecta, 2×10^9 kg of HB coma, and 1×10^{22} kg of HD 100546 disk in the 0.1–20 um particle size range. A number of things become clearer once this is noted. The Spitzer T1 ejecta measurements were extremely sensitive, revealing a number of new spectral features despite observing 10^3 times less material than was observed by ISO in HB. Also, the total amount of material released in the ejecta was only a small fraction, $\sim 10^{-4}$, of the mass of the dust in the ambient T1 coma. Even so, the emission from this dust was a good 25% of the total observed emission from the comet while the ejecta remained near the nucleus, because of the very large emission efficiency for small, crystalline dust particles. The amount of HB material in the ISO beam was a relatively small fraction (~1%) of the total dust mass in the coma ($\sim 1 \times 10^{11}$–1×10^{12} kg), but focused on the freshest and newest material emitted from the nucleus. The 1×10^{22} kg observed material in HD 100546 is not from a few comets, or even one giant comet. The amount of material observed is equivalent to the mass of $\sim 10^8$ typical JFC comets, or the mass of a Kuiper belt. The system appears to be a disk of material with a range of particle sizes and the process of planet formation going on nearby. Thus we can expect the presence of particles larger than 20 um with appreciable mass but low emitting surface area to mass ratio, so this is most likely a lower limit to the total mass present.

5.2. *Composition of the 3 systems—overview*

For an ~10 Myr old system with at least 10^8 comet's worth of mass spread out over many AU, in the process of disk clearing and planet building, it is quite striking that HD resembles HB closely in composition (as noted in the HD composition section above, and illustrated in the barchart of Fig. 5). As the HD material is located in a region analogous to the inner giant planet region of the PSN, this would seem to indicate that HB was also formed in the inner giant planet region. It is tempting to "date" HD as younger than HB and T1 based on the large amount of amorphous pyroxenes and PAHs, both primitive species, and the size distribution dominated by extremely small grains, implying little particle aggregation. We are given pause, however, by the unusually small amount of amorphous olivine, the lack of Fe-rich carbonates, and the evidence for nearby planet formation and disk clearing. HD is relatively well dated as a system of ~10 Myr age, more evolved than other Herbig Ae–Be stars by a few Myr (Grady et al., 2005). The giant planet cores in the Solar System are thought to have formed within 5 to 10 Myr (Boss, 2004), so by inference, HB is this age or younger. The HD 100546 Be9 V primary is of very unusual composition, of the "lambda Bootis" type (Acke and Waelkens, 2004). This type of star has the chemical peculiarity of having photospheric abundances in which C, N, O, and S are roughly solar

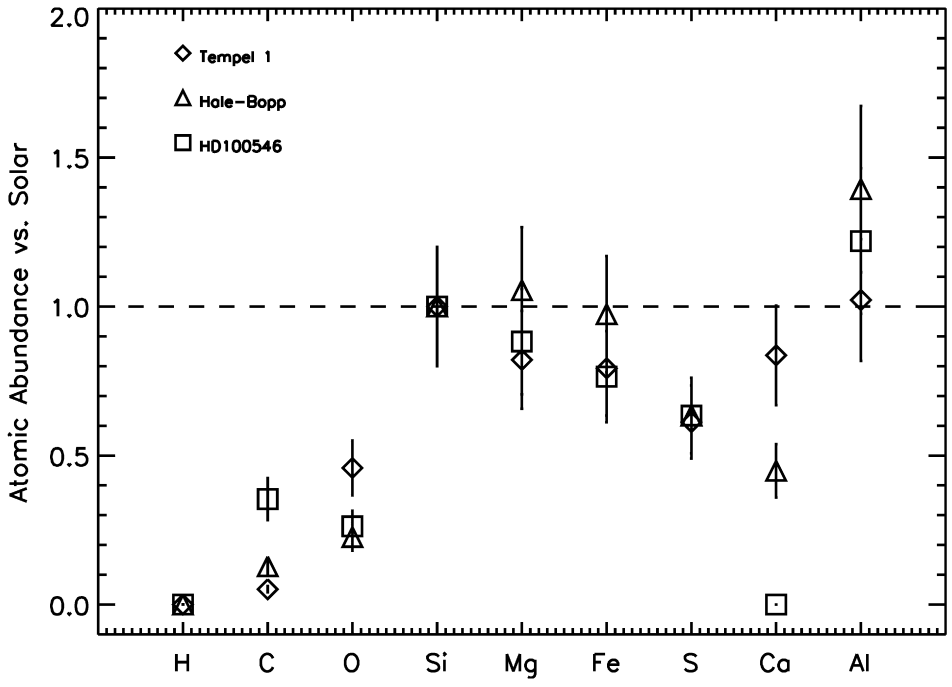

Fig. 6. *Elemental abundances for the 3 systems vs solar, assuming Si = 1.0.* 2σ error bars for the relative measures are ±20%. Diamonds—Tempel 1, squares—HD 100546, triangles—Hale–Bopp. The nominal solar value is denoted by the dashed line. The largest apparent differences are in the C, O, and Ca abundances. The C abundances may be affected by the ISO-SWS calibration (see text).

but metals are depleted. Given the chemical oddities in the photosphere, it is not too surprising that there might be some in the circumstellar disk as well. HD has also been noted as having an unusual mid-IR SED for an HBe system (Bouwman et al., 2003; Grady et al., 2005), with a huge IR excess due to abundant small dust grains. So the unusual silicate and carbonate abundances might be due to an unusual starting composition, or to the fortuitous circumstance of observing a system during the relatively brief active disk clearing phase after planetary core formation, when shock and collisional processing of nebular material is active (cf. Wyatt et al., 2007).

On the other hand, comparing HB and T1, the two Solar System bodies, a clear temporal progression can be seen. The silicates in T1 are all much more crystalline than in HB, and the amount of PAHs is reduced by a factor of 25. In contrast, HB's composition is closer to the mix of silicates and PAHs in the ISM than T1. The difference in the two comets cannot be due to differences in the location of formation, as HB originated in the denser and warmer giant planet region, where rates of processing would, if anything, be higher than in the trans-neptunian region where T1 formed, leading to a more processed body.

5.3. Composition of the 3 systems—materials expected in the PSN and YSOs

The range of temperatures of formation for the most stable common chemical compounds found in the PSN, comets, and YSOs is as follows. In general, the simple metal oxides, C grains, and CO are the most stable molecules and are observed in the atmospheres of asymptotic giant branch (AGB) stars at temperatures up to 2500 K. They are followed in stability by the silicates which condense in the outer atmospheres and thick winds of AGB stars at temperatures of 1000–1400 K. Next in stability are the phyllosilicates and native Fe/Fe–Ni metal, forming in the range 600–900 K. The carbonates form at 600–700 K and the sulfides are stable below ∼600 K. Water ice is stable at temperatures $\leqslant$200 K in vacuum, while the ices of methane, carbon monoxide, and carbon dioxide evaporate at much lower temperatures, below 100 K in vacuum.

This flowdown of materials assumes, of course, that they formed slowly as condensates from a gas where all pre-existing dust had been vaporized. Due to the survival of many types of pre-solar grains, we know this process did not occur entirely uniformly. Dynamic processes, such as mixing, shocks, and turbulence can create local non-homogeneities, complicating the situation. Stratification of materials and reaction processes are also expected, as the Sun, the energy source for the formation of materials, was located at the center of the system rather than spaced uniformly throughout. It was also a source of stochastic heating by high-energy photons. Despite these potential complications, the condensation sequence is still a useful construct to consider as a measure of the relative stability of individual minerals.

In the PSN, the dominant species, of course, was H_2. Thus the early PSN was a highly reducing environment. Any species not highly refractory and not already formed, like the metal oxides and silicates around AGB stars and novae, would be predominantly in the form of CH_4, C_2H_6, H_2O, H_2S, NH_3, etc. That is, simple molecules were the most abundant, and the majority of species were compounds of hydrogen. Some exceptions to this rule exist, such as the extremely stable N_2, CO and CO_2 molecules. Once formed in molecular clouds, they can last for long periods of time in reasonably quiescent (e.g., shock-free and/or low UV-field) environments. Carbon grains formed

of graphite-like lattices are also extremely stable once formed. Hydrogenation of the surface can occur, though, and some of this surface hydrogenation will lead to PAH formation.

There was little or no free O in the form of O_2 to perform the redox reactions so familiar to terrestrial and planetary geology. The most abundant oxidant available was instead sulfur, obtained from the labile H_2S molecule. The formation of sulfides from native Fe and Fe–Ni mixtures was an oxidation reaction. The fact that no sulfates have been found in primitive materials reflects the lack of reactive oxygen. Sulfates are the normal end product of oxidative attack on sulfide materials, but the oxidative attack on native Fe stopped at the sulfide level in the PSN. Carbonates, on the other hand, can be formed directly from CO_2, water, and silicates. The oxidation of the carbon and silicon by oxygen, and the binding of the oxygen in the component molecules, has already occurred.

In sum, the solid state species we expect to see in bulk in comets and YSOs is as follows:

- C in carbon grains, organic ices, and PAHs;
- O in silicates, oxides, and water;
- S in sulfides and H_2S;
- Si in silicates, generally in the form of olivines and pyroxenes;
- Fe in silicates, Fe–Ni grains and Fe–NiS_x;
- Mg in silicates, MgS, and MgO;
- Al, Ca in silicates and as simple oxides.

This closely corresponds to the range of materials making up the compositional model for the Spitzer observations of the DI experiment (Lisse et al., 2006), found by systematic fitting of laboratory mineral spectra to the T1 ejecta spectra, and of the species found in HB and HD 100546 in this work.

5.4. Compositional trends in the T1/HB/HD100546 spectra

The results from the new modeling raise a number of issues. Because the sample size (2 comets and 1 YSO) is so small, we present each as a question. Definitive answers are impossible for a small dataset with known selection biases. On the other hand, examination of the dataset can be used to suggest trends and processes that may be verified in future studies with a larger numbers of objects.

5.4.1. Do silicates change with system age?

The crystallinity and Fe/Mg composition balance of the silicates provides a high temperature, chemically robust record of the formation history of the cometary material. For example, pyroxenes are easier to modify thermally than olivines (Hallenbeck et al., 1998; Nuth and Johnson, 2006). From the DI experiment the T1 silicate composition is more than 80% crystalline, has an olivine:pyroxene ratio of about 1, and has relatively good equilibration between the Fe- and Mg-rich in both the olivine and pyroxene phases. The silicates in HD are a very simple system—only Mg-rich crystalline olivine, amorphous pyroxene, and some crystalline pyroxenes are present, with about 50% total crystalline material and an olivine:pyroxene ratio of about 1. The HB system seems intermediate between the two, with ∼67% crystalline olivines and pyroxenes, relatively more Fe/Ca/Mg-equilibrated pyroxenes, a goodly amount of amorphous olivine, but again only Mg-rich crystalline olivine. The silicate evidence implies that the dust in T1 has been most heavily processed of the three systems.

To test if the different apparent nature of the T1 silicates is due to the different spectral resolutions and sensitivities for the SWS and IRS instruments, we smoothed the T1 spectrum to match the "rounder" features of the ISO HB data. We recovered the same mix of materials as found for the unsmoothed data, including the Fe-rich silicates not found in HB. Also, the preliminary results of Stardust for Comet Wild 2, a Jupiter family comet (JFC) like T1, confirm the presence of Mg-rich olivines and Ca- and Fe-rich pyroxenes in the Wild 2 dust (Brownlee et al., 2006b).

If silicates were processed by annealing near the Sun, then this implies an efficient mechanism for transferring silicaceous dust from the inner Solar System to the K–E belt for some time after the Oort cloud comets such as HB formed in the giant planet region (Gail, 2004; Keller and Gail, 2004). However, efficient radial transport from the inner nebula should end at about the time of giant planet core formation, at ∼10 Myr (Boss, 2004). The density of material in the giant planet region was much higher than at the edges of the PSN in the K–E belt where JFCs formed. Thus, Oort cloud comets like HB, on the whole, probably formed before JFCs like T1. We can "date" the average Oort cloud comet at less than 10 Myr, the time estimated for the giant planet core formation—the giant planet planetesimals were formed first, before the giant planets themselves. This leaves the relatively short time between formation of the planetesimals and the first planet cores as the source of the difference in the silicates in T1 and HB, even when we also consider nebular shock processing and evolutionary processing due to repeated solar passages.

The shock theory of Harker and Desch (2002) argues that crystalline silicates should start forming at the time of giant planet core creation and growth. Shocks had only until the time of orbital ejection of the planetesimal into the Oort cloud to work on the material of HB. The material in the slower forming T1 could have been processed until the giant planets finished accreting. The existence of the primitive chondrules, which appear to have been formed from liquid phase solidification of molten PSN material, provides strong evidence for shocks in the PSN. If shocks formed the primitive chondrules and altered the silicaceous material in T1, then the mineral composition of JFCs like T1 should be closer to chondritic than Oort cloud comets like HB which formed in the pre-shock era. However, while there is good agreement between the T1 and C1 chondritic abundances, there is equally good agreement between the HB and the C1 abundances. The low Fe/Mg crystalline olivine ratio, low particle strength, and high porosity also argue for mainly thermal processing and against much shock processing of the material in T1, as suggested by Lisse et al. (2006). On the other hand, as noted above, shocks may very well be strongly processing the HD silicate material, reforming it into a mix of Mg-rich olivine and amorphous pyroxene. To have left

the other materials in the system with a comet-like composition while altering the highly refractory silicates takes some special conditions. It would seem to require destruction of the materials in the inner disk cavity ($r^* < 13$ AU) and efficient transport of the shock processed material into the edge of the disk at $r^* \sim 13$ AU, adding to and overwhelming the local, unprocessed, "native" silicate composition.

The Mg/Fe silicate equilibration seen in T1 could have occurred since cometary formation, in the repeated close passages by the Sun, building up a mantle of material substantially different from the bulk interior. This process would also appear to have caused an equilibration of the Mg/Fe abundance in the sulfide phases as well (Section 5.4.4). However, it is unlikely that Fe/Mg cation migration could occur at the low temperatures found in cometary bodies. It clearly has not in HB, while chemistry leading to carbonate and phyllosilicate formation has. Further, there is now abundant evidence from the DI mission that the average material on T1 was thermally processed to depths of less than 1 m (Groussin et al., 2007; A'Hearn et al., 2007) while the DI impactor ejected material from depths of 10–30 m deep. Barring any extensive reworking of the interior material by impact processing, we thus conclude that there was an exceptional amount of processing of nebular material in the PSN between the time of HB's formation and the end of the era of giant planet formation, when substantive inputs to the T1 composition would have ended.

5.4.2. Are PAHs as common in nebulae and comets as in the ISM?

PAHs, while not the major carriers of carbon in the Solar System and ISM (they are observable mainly due to their pronounced UV-driven fluorescence) are nevertheless important species chemically and useful tracers of processing in stellar environments. In the diffuse ISM, the abundance of PAHs vs silicates is 1–10%, orders of magnitudes higher than what is found in comets (Li and Draine, 2001; Li and Draine, 2007. On PAHs is comets, in preparation). This suggests that while PAHs could be part of the earliest material input into the PSN, they might have been removed or destroyed as the system evolves. Does the removal of PAHs begin as a molecular cloud core collapses into the protostellar disk, or does it happen later, as the central source turns on and irradiates the circumstellar material? The strong PAH signal in HD and many other YSOs (Sloan et al., 2005) argues that PAHs often survive infall and are destroyed later (e.g., photodissociated in the PSN after they emerge out of the sublimating ice mantles of dust grains).

The fact that other parts of the HD spectrum seem to match cometary spectra well has been used in the past to argue that PAHs should be common in comets. As mentioned in the HB compositional modeling section, the comet was found to be rich in simple organic species (Biver et al., 1999; Bockelée-Morvan et al., 2000), so it is not surprising that carbonaceous PAHs were found using the detailed modeling described in this work. Ionized PAHs are found in all 3 systems in this study, and are beginning to seem ubiquitous at the thousand ppm level, as the mid-IR spectra from two other comets observed by Spitzer also show evidence for PAHs (Lisse et al., 2007, in preparation). The markedly stronger emission features would seem to argue for much more PAH abundance in HD than HB, but the abundances in Tables 2 and 3 indicate they are at roughly the same abundance level, 2×10^{-2} molar ratio. This seeming contradiction can be resolved when the mechanism driving the PAH emission, UV pumping by the G2 V Sun or the Be9 V HD primary, rather than direct heating by stellar insolation, is accounted for. It is also important to note that the abundance level of PAHs in HD and HB is about the same as in the ISM, implying that PAHs can indeed survive infall and incorporation into young Solar System bodies.

The larger abundance of PAHs in HB compared to T1, about a factor of 25 (Lisse et al., 2006), appears to be a real effect, which we ascribe to the later time of formation of T1, as PAHs become gradually more scarce in the PSN as they are destroyed over time. As for the case of silicate processing, we believe we can rule out the effects of different formation locations. In the mixing scenario, PAHs would be destroyed more quickly in the giant planet region, where solar UV and molecular H_2 were much more abundant, than in the K–E belt. The PAHs in the giant planet region could easily have continued on the path of reduction to still smaller, saturated organics by photochemistry in the PSN. This process would have taken longer to perform in the relatively dark and diffuse K–E belt, allowing substantially more PAHs to survive intact there. The shock model would also argue for a more rapid destruction of PAHs in the dense PSN material of the giant planet region, which is capable of supporting stronger shocks than the sparse material in the K–E belt. The fact that we see a higher relative abundance of PAHs in HB than in T1 argues for an earlier age of formation for HB, as does the more primitive nature of the silicates.

5.4.3. Are carbonates and phyllosilicates present?

The presence of the minor carbonate and phyllosilicate species in YSOs or comets is an issue currently in much debate. Ceccarelli et al. (2002) and Chiavassa et al. (2005) found that half of the YSOs in their ISO Long Wavelength Spectrometer (LWS; Gry et al., 2003) study have carbonate emission. Recent work by Toppani et al. (2005) demonstrated that carbonates can form from gas-phase silica, water, and carbon dioxide, although at relatively high partial pressures versus those found in the PSN. Re-analysis of the IDP record has shown evidence for carbonate materials (Flynn et al., 2005). Comets are known to contain abundant water ice, carbon dioxide, and silicates, all which can react in the parent body to form carbonates and phyllosilicates in planetary environments. Also, there are no other likely, highly abundant sources of emission in the wavelength range 6.5–7.5 μm, where we find the carbonate peak.

On the other hand, the canonical wisdom holds that carbonates and phyllosilicates only form in the presence of liquid water. This would mean that liquid water must have been present in T1 and HB at some point, a finding surprising to many, although new work by Merk and Prialnik (2006) argues for abundant liquid water in KBOs during the era of formation due to heating by Al^{26}. Also, there is some controversy over the claim of carbonate detection by Ceccarelli et al. (2002) and Chiavassa et al. (2005). The emission features used to determine the presence

and amount of carbonates found in LWS spectra at 90–110 um are relatively broad and shallow. They depend highly on the continuum subtraction in many cases, and the results could be confused with emission lines due to silicates and phyllosilicates (e.g., Bouwman et al., 2003).

Definitive evidence for carbonates or phyllosilicates has yet to be found in the Stardust samples studied to date, which is worrisome. It is not clear at the time of this writing how much small number statistics, hot sample collection into aerogel, collection of mainly surface mantle (and thereby altered) material, or samples from a substantially younger comet affect the Stardust samples vs the Deep Impact experiment results; e.g., so far only the most refractory of species (silicates and sulfides) have been recovered intact in the terminal particles of the Stardust tracks; UV photodecomposition could transform carbonates in the surface layers of Comet Wild 2 into metal oxides and CO_2 (as occurs on Mars, where no carbonates are found, despite the prevalence of species and structures formed by aqueous water alteration of the surface material, similar to where carbonates are found terrestrially); or, as no obvious impact craters were found on the surface of Wild 2 (Brownlee et al., 2004), the bulk material of Comet Wild 2 may have undergone no substantial impact processing. With respect to the latter point, it should be kept in mind that Deep Impact sampled material from one place at depth on T1, located between two 300 m wide impact craters, where reworking of the comet has clearly occurred. It is quite possible that the T1 ejecta, while definitively from the interior of the comet, contains some additional species, along with the materials found in a young comet, due to impact driven chemical processing (Lisse et al., 2006).

Given this uncertain context, we find it telling that our model detects carbonates in the highly active and water-rich HB system and in T1 as well as in the HD YSO system, but only after we carefully removed the photospheric contribution. This gives us confidence that our model does not detect 'false positive' carbonates. One other point can be made from our modeling: the relationship (or lack thereof) between the parent silicates and daughter carbonate products. In HB, the carbonates are slightly Fe-rich, with a 6:5 ratio of siderite to magnesite, with about 15% abundance by surface area. For T1, the ratio is 5:3, with about 5% abundance. Both ratios mimic the pyroxene, but not the olivine, Fe:Mg ratios. For HD we find only Mg-rich carbonate at about 3% abundance, which agrees with the large preponderance of Mg-rich olivine, but not the relatively Fe-rich pyroxenes. The unusually large amount of amorphous pyroxene in HD may be a clue to unusual pyroxene chemistry in this system. Also, the effect of shocks and collisions on carbonate materials is unclear, although we would expect them to be relatively "unrefractory" vs the other species in our compositional mix, decomposing to a mix of carbon dioxide and metal oxide. More detailed IR observations of comets and YSO systems are clearly needed to answers these questions.

5.4.4. What can be learned from the sulfide mineralogy in the 3 systems?

Forming at ~600 K, sulfides have the promise of being extremely useful diagnostics of the local PSN environment (Keller et al., 2002). The major difference among the three systems is that HB and HD 100546 are much better fit by an Fe-rich sulfide component with stoichiometry $Fe_{0.9}Mg_{0.1}S$ as opposed to the $Fe_{0.5}Mg_{0.5}S$ found in the T1 ejecta. From this and the determination that HB and HD 100546 are less chemically evolved than T1, we infer that the less equilibrated sulfides are more primitive. Preliminary evidence from the Stardust mission is that the Comet 81P/Wild 2 sulfides occur in the form of non-stoichiometric FeS_x (with admixtures of Ni; Keller et al., 2006; Zolensky et al., 2006). This mineral system is currently poorly understood by ground based laboratory studies and as a consequence is not well supported in our model, but does appear to be more closely related to the Fe-rich ningerites found for HB and HD in this work. In addition, some quantity of S bearing molecules such as H_2S or SO_2 may not react with available metals and thus may not become incorporated in the dusty/icy aggregates that accrete to form the comets. Until better laboratory and Stardust measurements are made, the sulfide question will remain open.

6. Conclusions

1. The same model used to fit the T1 ejecta composition fit the HB and HD systems well. The model is based as much as possible on experimental observation and materials analysis of sample returns. Dominant features for the systems found in other models, like the dominance of Mg-rich olivines and water ice in HB and the presence of PAHs and Mg-rich olivines in HD, were reproduced.
2. Particle temperature and grain size effects must be included in the models to accurately determine compositional mineralogy with mid-IR spectra. The material in T1 yielded very different emission spectra when it was emitted naturally in large aggregates (ambient coma) or separated into a fine powder by the DI experiment (ejecta).
3. The detailed mid-IR spectra of the T1 ejecta, the Comet HB coma, and the HD nebula are qualitatively similar. However, there are important differences between the systems as well which allow for a comparative mineralogy study.
4. The material incorporated in HB appears to be less processed than that in T1, as determined from the differences in their crystalline silicate content. The relative abundance of PAHs in HB and in T1 can be explained by a net destruction over time of PAHs in the PSN, along with an earlier formation time for comets in the giant planet region vs the K–E belt.
5. Both comets contain carbonates and phyllosilicates, as does HD100546. The cometary carbonate Fe:Mg composition follows the pyroxene composition in the comet systems.
6. The HD SED can be explained by emission dominated by a single mix of material co-located at ~13 AU. The two different apparent temperature regimes are due to the presence of abundant hot refractory dust mixed with abundant sublimation cooled water ice particles.
7. The material composition of HD 100546 seems to be very similar to that of the two comet systems, with the exception of the absence of amorphous olivine and the superabun-

dance of amorphous pyroxene. The presence of abundant PAHs and water ice implies that there is little processing of the nebular material. The unusual silicate composition may be due to either a different starting composition for the HD nebula vs the PSN, or due to shock and collisional processing of material inside 13 AU caused by due to planet formation and disk clearing, followed by transport into the inner edge of the surrounding disk.

8. PAHs are found in all 3 systems studied. The abundance of PAHs in HB and HD is roughly the same, ∼2% vs the bulk, similar to the level seen in the ISM. T1 is depleted in PAHs, by a factor of 25.

Acknowledgments

The authors thank the members of the Deep Impact Spitzer team, and the Cornell IRS group for their help in preparing the Spitzer IRS T1 spectrum. The ISO SWS spectrum of HD 100546 was graciously provided by C. Waelkens, and the HB spectrum by J. Crovisier. We gratefully acknowledge helpful discussions of our work with S. Bajt, L. Keller, and L.A. McFadden. C.M. Lisse was supported by Spitzer GO grants, JPL contracts 1274400 and 1274485, in performing this work. J.A. Nuth was supported in part by NASA's Cosmochemistry program. A. Li is supported in part by the University of Missouri Summer Research Fellowship, the University of Missouri Research Board, the NASA/HST Theory Program, and the NASA/Spitzer Theory Program.

References

Acke, B., Waelkens, C., 2004. Chemical analysis of 24 dusty (pre-)main-sequence stars. Astron. Astrophys. 427, 1009–1017.

A'Hearn, M.F., and 32 colleagues, 2005. Deep Impact: A large-scale planetary experiment. Science 310, 258–264.

A'Hearn, M.F., and colleagues, 2007. Deep Impact and sample return. Earth Planets Space, submitted for publication.

Anders, E., Grevesse, N., 1989. Abundances of the elements—Meteoritic and solar. Geochim. Cosmochim. Acta 53, 197–214.

Asplund, M., Grevesse, N., Sauval, A.J., 2005. The solar chemical composition. In: Bash, F.N., Barnes, T.G. (Eds.), Cosmic Abundances as Records of Stellar Evolution and Nucleosynthesis. In: ASP Conf. Series, vol. 336. ASP, San Francisco, pp. 25–39.

Biver, N., and 13 colleagues, 1999. Long-term evolution of the outgassing of Comet Hale–Bopp from radio observations. Earth Moon Planets 78, 5–11.

Biver, N., and 22 colleagues, 2002. The 1995–2002 long-term monitoring of Comet C/1995 O1 (Hale Bopp) at radio wavelength. Earth Moon Planets 90, 5–14.

Bockelee-Morvan, D., Brooke, T.Y., Crovisier, J., 1995. On the origin of the 3.2–3.6 um emission feature in comets. Icarus 116, 18–39.

Bockelée-Morvan, D., and 17 colleagues, 2000. New molecules found in Comet C/1995 O1 (Hale–Bopp). Investigating the link between cometary and interstellar material. Astron. Astrophys. 353, 1101–1114.

Bockelée-Morvan, D., Gautier, D., Hersant, F., Huré, J.-M., Robert, F., 2002. Turbulent radial mixing in the solar nebula as the source of crystalline silicates in comets. Astron. Astrophys. 384, 1107–1118.

Boss, A.P., 2004. Evolution of the solar nebula. VI. Mixing and transport of isotopic heterogeneity. Astrophys. J. 616, 1265–1277.

Bouwman, J., de Koter, A., Dominik, C., Waters, L.B.F.M., 2003. The origin of crystalline silicates in the Herbig Be star HD 100546 and in Comet Hale–Bopp. Astron. Astrophys. 401, 577–592.

Bradley, J., 2002. The astromineralogy of interplanetary dust particles. In: Henning, T.K. (Ed.), Astromineralogy. In: Lecture Notes in Physics, vol. 609. Springer-Verlag, Berlin, pp. 217–235.

Bradley, J.P., 2003. Interplanetary dust particles. In: Davis, A.M., Holland, H.D., Turekian, K.K. (Eds.), Treatise on Geochemistry. Elsevier, Amsterdam, pp. 689–711.

Bregman, J.D., Witteborn, F.C., Allamandola, L.J., Campins, H., Wooden, D.H., Rank, D.M., Cohen, M., Tielens, A.G.G.M., 1987. Airborne and groundbased spectrophotometry of Comet P/Halley from 5–13 micrometers. Astron. Astrophys. 187, 616–620.

Brownlee, D.E., and 11 colleagues, 2004. Surface of young Jupiter family Comet 81P/Wild 2: View from the Stardust spacecraft. Science 304, 1764–1769.

Brownlee, D.E., Flynn, G., Hörz, F., Keller, L., McKeegan, K., Sandford, S., Tsou, P., Zolensky, M.E., 2006a. Comet samples returned by the Stardust mission. Lunar Planet. Sci. 37. Abstract 2286.

Brownlee, D.E., and the Stardust Team, 2006b. Laboratory studies of comet samples returned by Stardust. Bull. Am. Astron. Soc. 38, 2302B.

Ceccarelli, C., Caux, E., Tielens, A.G.G.M., Kemper, F., Waters, L.B.F.M., Phillips, T., 2002. Discovery of calcite in the solar type protostar NGC 1333-IRAS 4. Astron. Astrophys. 395, L29–L33.

Chiavassa, A., Ceccarelli, C., Tielens, A.G.G.M., Caux, E., Maret, S., 2005. The 90–110 micron dust feature in low to intermediate mass protostars: Calcite? Astron. Astrophys. 432, 547–557.

Clairemidi, J., Brechignac, P., Moreels, G., Pautet, D., 2004. Tentative identification of pyrene as a polycyclic aromatic molecule in UV spectra of Comet P/Halley. Planet. Space Sci. 52, 761–772.

Clark, B.C., Mason, L.W., Kissel, J., 1987. Systematics of the CHON and other light element particle populations in Comet P/Halley. Astron. Astrophys. 187, 779–784.

Crovisier, J., Leech, K., Bockelee-Morvan, D., Brooke, T.Y., Hanner, M.S., Altieri, B., Keller, H.U., Lellouch, E., 1997. The spectrum of Comet Hale–Bopp (C/1995 O1) observed with the Infrared Space Observatory at 2.9 AU from the Sun. Science 275, 1904–1907.

Crovisier, J., and 13 colleagues, 2000. The thermal infrared spectra of Comets Hale–Bopp and 103P/Hartley 2 observed with the Infrared Space Observatory. In: Sitko, M.L., Sprague, A.L., Lynch, D.K. (Eds.), Thermal Emission Spectroscopy and Analysis of Dust, Disks, and Regoliths. In: ASP Conf. Series, vol. 196. ASP, San Francisco, pp. 109–117.

Dello Russo, N., Mumma, M.J., DiSanti, M.A., Magee-Sauer, K., Novak, R., Rettig, T.W., 2000. Water production and release in Comet C/1995 O1 Hale–Bopp. Icarus 143, 324–333.

Dutrey, A., Guilloteau, S., 2004. Observations of circumstellar disks. Astrophys. Space Sci. 292, 407–418.

Encrenaz, T., d'Hendecourt, L., Puget, J.L., 1988. The interpretation of the 3.2–3.5 micron emission feature in the spectrum of Comet P/Halley. Astron. Astrophys. 207, 162–173.

Fernandez, Y.R., Lisse, C.M., Kelley, M.S., Dello Russo, N., Tokunaga, A.D., Woodward, C.E., Wooden, D.H., 2007. Near-infrared light curve of Comet 9P/Tempel 1 during Deep Impact. Icarus 187, 220–227.

Flynn, G.J., Keller, L.P., Sutton, S.R., 2005. Dust in planetary systems. In: Proceedings of the Conference held 26 to 28 September 2005, Kaua'i, Hawaii, Lunar and Planetary Institute Contribution No. 1280, p. 48.

Forrest, W.J., and 20 colleagues, 2004. Mid-infrared spectroscopy of disks around classical T Tauri stars. Astrophys. J. Suppl. 154, 443–447.

Gail, H.-P., 2004. Radial mixing in protoplanetary accretion disks. IV. Metamorphosis of the silicate dust complex. Astron. Astrophys. 413, 571–591.

Grady, C.A., and 28 colleagues, 2001. The disk and environment of the Herbig Be star HD 100546. Astron. J. 122, 3396–3406.

Grady, C.A., Woodgate, B., Heap, S.R., Bowers, C., Nuth III, J.A., Herczeg, G.J., Hill, H.G.M., 2005. Resolving the inner cavity of the HD 100546 disk: A candidate young planetary system? Astrophys. J. 620, 470–480.

Groussin, O., A'Hearn, M.F., Li, J.-Y., Thomas, P.C., Sunshine, J.M., Lisse, C.M., Meech, K.J., Farnham, T.L., Feaga, L.M., Delamere, W.A., 2007. Surface temperature of the nucleus of Comet 9P/Tempel 1. Icarus 187, 16–25.

Gry, C., and 17 colleagues, 2003. The ISO Handbook, vol. III, LWS—The Long Wavelength Spectrometer. ESA, Noordwijk. ESA SP-1262.

Hallenbeck, S.L., Nuth, J.A., Daukantas, P.L., 1998. Mid-infrared spectral evolution of amorphous magnesium silicate smokes annealed in vacuum: Comparison to cometary spectra. Icarus 131, 198–209.

Hanner, M.S., Lynch, D.K., Russell, R.W., 1994. The 8–13 micron spectra of comets and the composition of silicate grains. Astrophys. J. 425, 274–285.

Hanner, M.S., Brooke, T.Y., Tokunaga, A.T., 1998. 8–13 micron spectroscopy of young stars. Astrophys. J. 502, 871–882.

Harker, D.E., Desch, S.J., 2002. Annealing of silicate dust by nebular shocks at 10 AU. Astrophys. J. 565, L109–L112.

Harker, D.E., Wooden, D.H., Woodward, C.E., Lisse, C.M., 2002. Grain properties of Comet C/1995 O1 (Hale–Bopp). Astrophys. J. 580, 579–597.

Harker, D.E., Woodward, C.E., Wooden, D.H., 2005. The dust grains from 9P/Tempel 1 before and after the encounter with Deep Impact. Science 310, 278–280.

Hörz, F., Zolensky, M.E., Bernhard, R.P., See, T.H., Warren, J.L., 2000. Impact features and projectile residues in aerogel exposed on Mir. Icarus 147, 559–579.

Houck, J., and 33 colleagues, 2004. The Infrared Spectrograph (IRS) on the Spitzer Space Telescope. Astrophys. J. Suppl. 154, 18–24.

Hu, J.Y., The, P.S., de Winter, D., 1989. Photometric and spectroscopic study of three candidate Herbig Ae/Be stars—HD 37411, HD 100546, and HD 104237. Astron. Astrophys. 208, 213–218.

Huebner, W., Benkoff, 1999. From coma abundances to nucleus composition. Space Sci. Rev. 90, 117–130.

Jessberger, E.K., Christofordis, A., Kissel, J., 1988. Aspects of the major element composition of Halley's dust. Nature 322, 691–695.

Jewitt, D.C., Matthews, H., 1999. Particulate mass loss from Comet Hale–Bopp. Astron. J. 117, 1056–1062.

Joswiak, D.J., Brownlee, D.E., 2006. Non-GEMS silicate glasses in chondritic porous interplanetary dust particles. Lunar Planet. Sci. 37. Abstract 2190.

Keller, Ch., Gail, H.-P., 2004. Radial mixing in protoplanetary accretion disks. VI. Mixing by large-scale radial flows. Astron. Astrophys. 415, 1177–1185.

Keller, L.P., Hony, S., Bradley, J.P., Molster, F.J., Waters, L.B.F.M., Bouwman, J., de Koter, A., Brownlee, D.E., Flynn, G.J., Henning, T., Mutschke, H., 2002. Identification of iron sulfide grains in protoplanetary disks. Nature 417, 148–150.

Keller, L.P., and 23 colleagues, 2006. Infrared, UV/VIS and Raman spectroscopy of Comet Wild 2 samples returned by the Stardust mission. Lunar Planet. Sci. 37. Abstract 2062.

Kessler, M., Mueller, T.G., Leech, K., Arviset, C., Garcia-Lario, P., Metcalfe, L., Pollock, A., Prusti, T., Salama, A., 2003. The ISO Handbook, vol. I, ISO—Mission and Satellite Overview. ESA, Noordwijk. ESA SP-1262.

Küppers, M., and 40 colleagues, 2005. A large dust/ice ratio in the nucleus of Comet 9P/Tempel 1. Nature 437, 987–990.

Leech K., and 16 colleagues, 2003. The ISO Handbook, vol. V, SWS—The Short Wavelength Spectrometer. ESA, Noordwijk. ESA SP-1262.

Lellouch, E., Crovisier, J., Lim, T., Bockelee-Morvan, D., Leech, K., Hanner, M.S., Altieri, B., Schmitt, B., Trotta, F., Keller, H.U., 1998. Evidence for water ice and estimate of dust production rate in Comet Hale–Bopp at 2.9 AU from the Sun. Astron. Astrophys. 339, L9–L12.

Li, A., Draine, B.T., 2001. Infrared emission from interstellar dust. II. The diffuse interstellar medium. Astrophys. J. 554, 778–802.

Li, A., Greenberg, M., 1998. From interstellar dust to comets: Infrared emission from Comet Hale–Bopp (C/1995 O1). Astrophys. J. 498, L83–L87.

Lisse, C.M., 2002. On the role of dust mass loss in the evolution of comets and dusty disk systems. Earth Moon Planets 90, 497–506.

Lisse, C.M., A'Hearn, M.F., Hauser, M.G., Kelsall, T., Lien, D.J., Moseley, S.H., Reach, W.T., Silverberg, R.F., 1998. Infrared observations of comets by COBE. Astrophys. J. 496, 971–991.

Lisse, C.M., and 14 colleagues, 1999. Infrared observations of dust emission from Comet Hale–Bopp. Earth Moon Planets 78 (1/3), 251–257.

Lisse, C.M., Fernandez, Y.R., A'Hearn, M.F., Peschke, S.B., 2002. A search for trends in cometary dust emission. In: Green, S.F., Williams, I.P., McDonnell, J.A.M. (Eds.), Dust in the Solar System and Other Planetary Systems. In: COSPAR Colloquia Series, vol. 15. Pergamon, Oxford, pp. 259–268.

Lisse, C.M., and 16 colleagues, 2006. Spitzer spectral observations of the Deep Impact ejecta. Science 313, 635–640.

Liu, W.M., Hinz, P.M., Meyer, M.R., Mamajek, E.E., Hoffmann, W.F., Hora, J.L., 2003. A resolved circumstellar disk around the Herbig Ae star HD 100546 in the Thermal Infrared. Astrophys. J. 598, L111–L114.

Malfait, K., Waelkens, C., Waters, L.B.F.M., Vandenbussche, B., Huygen, E., de Graauw, M.S., 1998. The spectrum of the young star HD 100546 observed with the Infrared Space Observatory. Astron. Astrophys. 332, L25–L28.

Megeath, S.T., Hartmann, L., Luhman, K.L., Fazio, G.G., 2005. Spitzer/IRAC photometry of the eta Chameleontis association. Astrophys. J. 634, L113–L116.

Melosh, H.J., 1989. Impact Cratering: A Geologic Process. In: Oxford Monographs on Geology and Geophysics, vol. 11. Clarendon Press, Oxford. And references therein.

Merk, R., Prialnik, D., 2006. Combined modeling of thermal evolution and accretion of trans-neptunian objects—Occurrence of high temperatures and liquid water. Icarus 183, 283–295.

Min, M., Hovenier, J.W., de Koter, A., Waters, L.B.F.M., Dominik, C., 2005. The composition and size distribution of the dust in the coma of Comet Hale Bopp. Icarus 179, 158–173.

Moreels, G., Clairemidi, J., Hermine, P., Brechignac, P., Rousselot, P., 1994. Detection of a polyaromatic molecules in Comet P/Halley. Astron. Astrophys. 282, 643–656.

Nuth, J.A., Johnson, N.M., 2006. Crystalline silicates in comets: How did they form? Icarus 180, 243–250.

Nuth, J.A., Hill, H.G.M., Kletetschka, G., 2000. Determining the ages of comets from the fraction of crystalline dust. Nature 406, 275–276.

Sloan, G.C., and 18 colleagues, 2005. Mid-infrared spectra of polycyclic aromatic hydrocarbon emission in Herbig Ae/Be stars. Astrophys. J. 632, 956–963.

Sugita, S., and 22 colleagues, 2005. Subaru Telescope observations of Deep Impact. Science 310, 274–278.

Sunshine, J.S., and 21 colleagues, 2006. Water ice on the surface of Comet Tempel 1. Science 311, 1453–1455.

Toppani, A., Robert, F., Libourel, G., de Donato, P., Barres, O., D'Hendecourt, L., Ghanbaja, J., 2005. A 'dry' condensation origin for circumstellar carbonates. Nature 437, 1121–1124.

Toth, I., Lisse, C.M., 2006. On the rotational breakup of cometary nuclei and Centaurs. Icarus 181, 162–177.

van den Ancker, M.E., The, P.S., Tjin A Djie, H.R.E., Catala, C., de Winter, D., Blondel, P.F.C., Waters, L.B.F.M., 1997. Hipparcos data on Herbig Ae/Be stars: An evolutionary scenario. Astron. Astrophys. 324, L33–L36.

Waelkens, C., Malfait, K., Waters, L.B.F.M., 1997. Comet Hale–Bopp, circumstellar dust, and the interstellar medium. Earth Moon Planets 79 (1/3), 265–274.

Weidenschilling, S.J., 1997. The origin of comets in the solar nebula: An unified model. Icarus 127, 290–306.

Weinberger, A.J., Becklin, E.E., Schneider, G., 2003. In: Deming, D., Seager, S. (Eds.), Scientific Frontiers in Research on Extrasolar Planets. In: ASP Conference Series, vol. 294. ASP, San Francisco, pp. 253–256.

Werner, M., and 25 colleagues, 2004. The Spitzer Space Telescope mission. Astrophys. J. Suppl. 154, 1–9.

Williams, D.M., Mason, C.G., Gehrz, R.D., Jones, T.J., Woodward, C.E., Harker, D.E., Hanner, M.S., Wooden, D.H., Witteborn, F.C., Butner, H.M., 1997. Measurement of submicron grains in the coma of Comet Hale–Bopp C/1995 O1 during 1997 February 15–20 UT. Astrophys. J. 489, L91–L94.

Womack, M., Wyckoff, S., Ziurys, L.M., 1992. Observational constraints on solar nebula nitrogen chemistry. Astrophys. J. 401, 728–735.

Wooden, D.H., Harker, D.E., Woodward, C.E., Butner, H.M., Koike, C., Witteborn, F.C., McMurtry, C.W., 1999. Silicate mineralogy of the dust in the inner coma of Comet C/1995 O1 (Hale–Bopp) pre- and post-perihelion. Astrophys. J. 517, 1034–1058.

Wooden, D.H., Butner, H.M., Harker, D.E., Woodward, C.E., 2000. Mg-rich silicate crystals in Comet Hale–Bopp: ISM relics or solar nebula condensates? Icarus 143, 126–137.

Wyatt, M.C., Smith, R., Greaves, J.S., Beichman, C.A., Bryden, G., Lisse, C.M., 2007. Transience of hot dust around Sun-like stars. Astrophys. J., in press. astro-ph#0610102.

Zolensky, M., and 13 colleagues, 2006. Mineralogy and petrology of Comet Wild 2 nucleus samples. Lunar Planet. Sci. 37. Abstract 1203.